# The pancreas anatomy conditions the origin and properties of resident macrophages

Boris Calderon,[1] Javier A. Carrero,[1] Stephen T. Ferris,[1] Dorothy K. Sojka,[2] Lindsay Moore,[1] Slava Epelman,[3] Kenneth M. Murphy,[1,4] Wayne M. Yokoyama,[1,2,4] Gwendalyn J. Randolph,[1] and Emil R. Unanue[1]

[1]Department of Pathology and Immunology; [2]Division of Rheumatology and [3]Division of Cardiology, Department of Medicine; and [4]Howard Hughes Medical Institute; Washington University School of Medicine in St. Louis, St. Louis, MO 63110

**We examine the features, origin, turnover, and gene expression of pancreatic macrophages under steady state. The data distinguish macrophages within distinct intrapancreatic microenvironments and suggest how macrophage phenotype is imprinted by the local milieu. Macrophages in islets of Langerhans and in the interacinar stroma are distinct in origin and phenotypic properties. In islets, macrophages are the only myeloid cells: they derive from definitive hematopoiesis, exchange to a minimum with blood cells, have a low level of self-replication, and depend on CSF-1. They express *Il1b* and *Tnfa* transcripts, indicating classical activation, M1, under steady state. The interacinar stroma contains two macrophage subsets. One is derived from primitive hematopoiesis, with no interchange by blood cells and alternative, M2, activation profile, whereas the second is derived from definitive hematopoiesis and exchanges with circulating myeloid cells but also shows an alternative activation profile. Complete replacement of islet and stromal macrophages by donor stem cells occurred after lethal irradiation with identical profiles as observed under steady state. The extraordinary plasticity of macrophages within the pancreatic organ and the distinct features imprinted by their anatomical localization sets the base for examining these cells in pathological conditions.**

CORRESPONDENCE
Emil R. Unanue:
unanue@wustl.edu

Abbreviations used: B6, C57BL/6; HSC, hematopoietic stem cell; ILC, innate lymphoid cell; LLO, listeriolysin O; NOD, nonobese diabetic; pDC, plasmacytoid DC; PLN, pancreatic LN.

Macrophages, different sets of DCs, and various innate lymphoid cells (ILCs) inhabit all tissues. Many are normal steady-state residents, whereas others turnover from the circulation (Merad et al., 2013; Spits et al., 2013; Epelman et al., 2014a). These various tissue-resident myeloid cells participate in defenses against pathogens and in the physiology and homeostasis of the tissue, as well as in important pathological states. Concerning macrophages, their heterogeneity has been found in several organs: macrophages may derive from primitive hematopoiesis in the yolk sac or from definitive hematopoiesis that develops first in the embryonic liver and later in BM (Ginhoux et al., 2010; Gautier et al., 2012; Hoeffel et al., 2012; Schulz et al., 2012; Guilliams et al., 2013; Yona et al., 2013; Epelman et al., 2014b). Macrophages also have a spectrum of activation states, with different gene signatures. The classical activation state, M1, was defined in the response to IFN-γ, whereas the alternative activation program, M2, was defined in the response to IL-4 (Sica and Mantovani, 2012; Gordon et al., 2014; Murray et al., 2014). Indeed, there are gene signatures that define each set. However, there is also a range of gene expression programs among macrophages in response to various stimuli, indicating a spectrum of activation states (Murray et al., 2014). Based on the expression of typical genes for each state, we refer to the macrophage activation profiles as M1 and M2, but being well aware of their heterogeneity. Examples of resident macrophages with an M2 profile are found in the testis and heart (Pinto et al., 2012; DeFalco et al., 2014).

The pancreas consists of two very different cellular components, the exocrine component (acinar glands) that secretes digestive enzymes into the intestine and the endocrine component

S. Epelman's present address is Peter Munk Cardiac Centre, Toronto General Hospital, University of Toronto, Toronto, Ontario M5G 1L7, Canada.

© 2015 Calderon et al. This article is distributed under the terms of an Attribution–Noncommercial–Share Alike–No Mirror Sites license for the first six months after the publication date (see http://www.rupress.org/terms). After six months it is available under a Creative Commons License (Attribution–Noncommercial–Share Alike 3.0 Unported license, as described at http://creativecommons.org/licenses/by-nc-sa/3.0/).

The Rockefeller University Press $30.00
J. Exp. Med. 2015 Vol. 212 No. 10 1497–1512
www.jem.org/cgi/doi/10.1084/jem.20150496



The Journal of Experimental Medicine

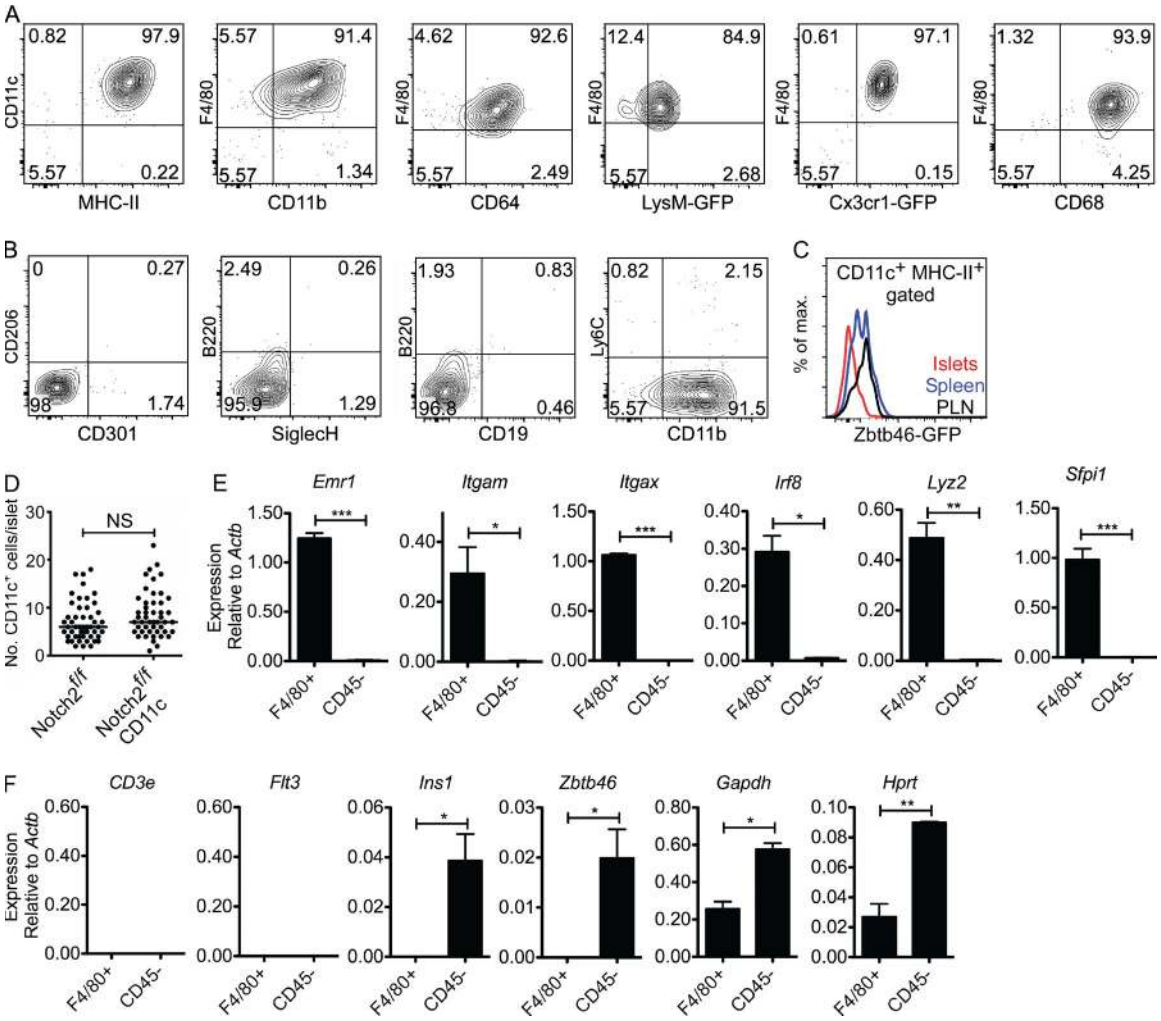


**Figure 1. Islet-resident leukocyte profile under steady state.** Islets from 8-wk-old B6 mice were analyzed by flow cytometry by gating on single CD45+ cells (see Fig. S1). (A and B) Islet-resident myeloid cells were cell surface positive for CD11c, MHC-II, F4/80, CD11b, CD64, lysozyme (LyzM)-GFP, $CX_3CR1$-GFP, and CD68 (A) and negative for CD206, CD301, B220, SiglecH, CD19, and Ly6C (B). Data are representative of six independent experiments. LyzM and $CX_3CR1$ were examined in LyzM-GFP and $CX_3CR1$-GFP reporter mice. (C) Expression of GFP in CD45+ CD11c+ MHC-II+ gated myeloid cells from islets, spleen, and PLNs of Zbtb46-GFP reporter mice. Data are representative of three independent experiments. (D) Shown is the number of myeloid cells (CD11c+) in whole islets isolated from $Notch2^{f/f}$ CD11c-cre reporter mice. Each dot represents the number of CD11c+ cells per individual islet, and bars indicate the median. Data are representative of two independent experiments evaluating 50 islets per group. (E and F) RT-PCR evaluation on sorted islet-resident macrophages (F4/80+) and the nonleukocyte compartment including endocrine and endothelial cells (CD45−) for the expression of leukocyte and nonleukocyte genes. Data are pooled from three independent experiments using 10 mice per sort. Bars indicate the mean ± SEM. P-values were calculated using unpaired Student's *t* test: *, $P < 0.05$; **, $P < 0.01$; ***, $P < 0.001$; NS, $P \geq 0.05$. Sample size included two to three samples per experimental group.

(islets of Langerhans) that secretes hormones into the blood stream. The pancreatic myeloid cells were first defined by immunohistochemistry using the F4/80 antigen, a marker highly expressed on macrophages (Hume et al., 1984). In the islets, myeloid cells were examined mainly in the context of mouse models of type 1 and type 2 diabetes (Ehses et al., 2007; Calderon et al., 2008; Melli et al., 2009; Westwell-Roper et al., 2014). Subsequent studies classified them as macrophages or DCs (Calderon et al., 2014). We recently reported that the intra-islet myeloid cells in the nonobese diabetic (NOD) mouse were composed mostly of F4/80+ macrophage with a few DCs of the CD103+ DC subset (Ferris et al., 2014). These were in intimate contact with blood vessels, projected extensions into their lumen, captured β cell–derived secretory granules, and had antigen-presenting capacity (Calderon et al., 2008; Mohan et al., 2010; Ferris et al., 2014). Mouse models of type 2 diabetes showed changes of islet macrophages to a proinflammatory profile (M1; Cucak et al., 2014; Westwell-Roper et al., 2014). Concerning the exocrine pancreas, macrophages were examined mostly in pathological situations (inflammation after ductal ligation, carbon tetrachloride–induced pancreatitis, and experimental pancreatic cancer)

and limited studies under steady state (Yin et al., 2011; Ino et al., 2014; Xiao et al., 2014).

Here we examine the life history of the endocrine and exocrine pancreatic phagocytes in the C57BL/6 (B6) mouse under steady state (noninflammatory conditions). We find differences between the two insofar as their embryonic origin and their M1/M2 profiles. These differences are maintained even when the resident macrophages are replaced by BM stem cells after genotoxic insult. Thus, the pancreas anatomy dictates the biology of the macrophage in very specific ways.

## RESULTS

### The islet-resident leukocytes

Studies have varied on the nature of the islet-resident myeloid cells in nondiabetic mouse strains and in the NOD mouse (reviewed in Calderon et al. [2014]). These differences may be caused by the techniques used for islet isolation. The degree of contamination of the islet preparation with stromal myeloid cells is of considerable importance because the islets represent a small percentage of the total pancreatic mass (Fig. S1 describes the technical approach used to evaluate islet cells). Direct microscopy of islets has shown the presence of myeloid $CD11c^+$ cells closely associated with the intra-islet vessels in small numbers, around 10 per islet (Calderon et al., 2008). Because of the expression of CD11c, several laboratories, including ours, initially defined them as DCs, but further evaluation shows them to be $F4/80^+$ $CD11c^+$ macrophages (Ferris et al., 2014).

We classified ∼98% of the islet-resident $CD45^+$ cells as macrophages based on surface marker and gene expression patterns. These cells had high expression of CD11c, MHC-II, F4/80, CD11b, CD64, lysozyme, $CX_3CR1$, and CD68 (Fig. 1 A). Islet macrophages were negative for mannose receptor 1 (*Mrc1*; CD206) and macrophage galactose-type C-type lectin (*Mgl1/2*; CD301; Fig. 1 B). DCs, plasmacytoid DCs (pDCs), B cells, $Ly6C^{hi}$ monocytes, and neutrophils were undetectable in islets (Fig. 1 B and Fig. S1 A). Further validation of the absence of DCs was established using the *Zbtb46*-GFP reporter mouse. (*Zbtb46* is a transcription factor expressed in DCs but not in macrophages, monocytes, or pDCs [Meredith et al., 2012; Satpathy et al., 2012].) Islets did not contain $CD45^+$ $Zbtb46^+$ cells (Fig. 1 C). Also, islets of the $Notch2^{f/f}$ CD11c-cre mouse showed normal number of macrophages (Fig. 1 D). Notch2 plays an essential role in $CD11b^+$ DC development in the gut and spleen (Lewis et al., 2011; Satpathy et al., 2013).

RT-PCR of flow cytometry–sorted islet macrophages showed expression of *Emr1*, *Itgam*, *Itgax*, *Irf8*, *Lyz2*, and *Sfpi1* (Fig. 1 E). *CD3e* was negative, making the point of the absence of T cells in the islets. *Flt3* and *Zbtb46* were not detected, confirming the lack of DCs in the $CD45^+$ $F4/80^+$ islet cells (Fig. 1 F). *Ins1* and *Zbtb46* were identified in the $CD45^-$ population composed of β cells and endothelial cells; the latter are known to express *Zbtb46* at low levels (Satpathy et al., 2012). In sum, the myeloid cell in the islets of Langerhans of the B6 mouse is a macrophage; no other discernible leukocyte subset is present under steady state (Table 1).

**Table 1.** Pancreatic macrophage profile under steady state

| Expression marker | Islet macrophage | Stroma $CD206^+$ macrophage | Stroma $CD206^-$ macrophage |
|---|---|---|---|
| F4/80 | + | + | + |
| CD11b | + | + | + |
| CD11c | + | + | + |
| MHC-II | + | +/− | + |
| CD64 | + | + | + |
| CD68 | + | + | + |
| LyzM | + | + | + |
| Cx3cr1 | + | +/− | +/− |
| CD206 | − | + | − |
| CD301 | − | + | − |
| Ly6C | − | − | − |
| CD103 | − | − | − |
| Zbtb46 | − | − | − |
| Il1b | + | − | − |
| Tnfa | + | − | − |
| Nos2 | − | − | − |
| Arg1 | − | +/− | +/− |
| Il10 | − | + | − |
| Ym1 | − | − | + |
| Fizz1 | − | + | + |

+, high expression; +/−, low expression; −, negative expression.

### The leukocytes of the exocrine pancreas

The leukocytes of the exocrine pancreas (pancreatic stroma) were heterogeneous and comprised three major sets (Fig. 2 A). The first set ($F4/80^+$ $CD11b^+$ in Fig. 2 A) represented ∼40% of the stromal leukocytes: although all expressed $CD11c^+$, only ∼60% were MHC-$II^+$, 40% expressed $CX_3CR1$ (Fig. 2 C), and half expressed CD206 and CD301 (Fig. 2 D). *Zbtb46*-GFP expression was negative. The second myeloid subset ($CD11b^+$ $F4/80^-$) represented ∼15% of all $CD45^+$ cells and contained two subsets: one consistent with DCs ($CD11c^+$ MHC-$II^+$ $Zbtb46^+$) and the second with monocytes ($Ly6C^+$ and $CX_3CR1^+$; Fig. 2, A–C). The third subset ($F4/80^-$ $CD11b^-$) represented ∼40% of the stromal leukocytes (Fig. 2, A–C). This group contained a variety of cells: ∼30% DCs ($CD11c^+$ MHC-$II^+$, of which ∼45% of them expressed CD103 and ∼75% expressed Zbtb46), ∼30% B cells (MHC-$II^+$ $CD19^+$ $B220^+$), ∼23% T cells (CD4 and CD8), and ∼15% ILCs (IL-17Rα$^+$ $CD3e^-$ cells previously described [Clark et al., 2007; Sojka et al., 2014]; Fig. S2). Overall, the stroma showed a complex leukocyte profile composed of macrophages, DCs, monocytes, B cells, T cells, and ILCs.

The expression of MHC-II on islet and stromal macrophages suggests they may be APCs. This has been proven to be the case only on islet macrophages (reviewed in Calderon et al. [2014]). We examined islet and stromal macrophages ($CD206^+$ and $CD206^-$) in a known assay system using listeriolysin O (LLO) protein (which requires processing) or the LLO peptide 190–210 (which only requires availability of

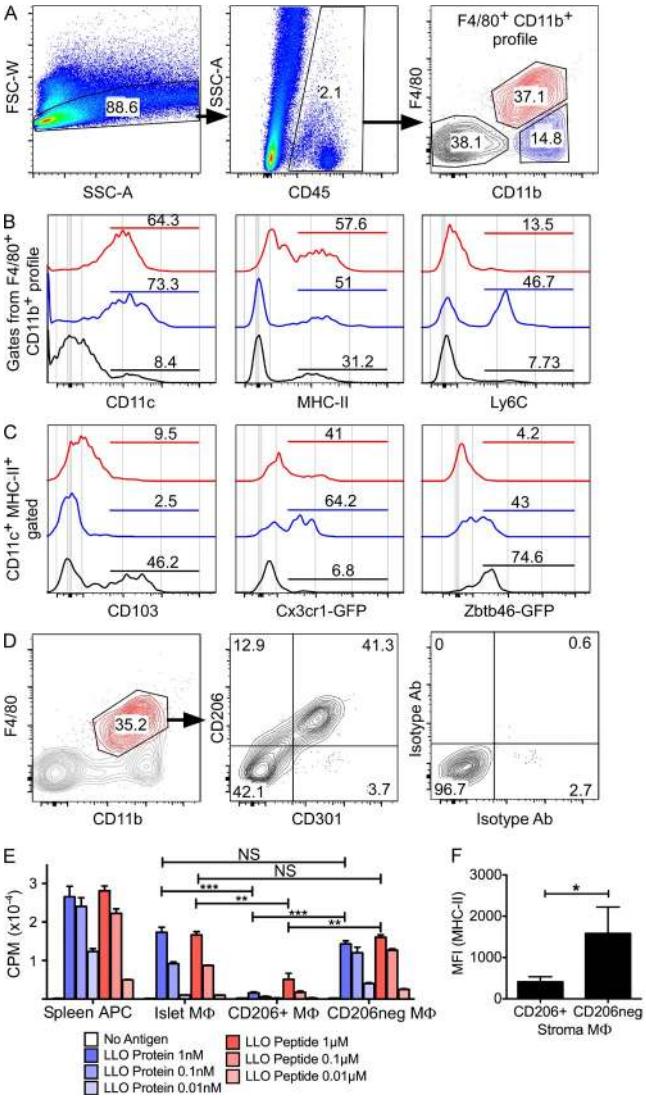


**Figure 2. Exocrine pancreas leukocyte profile under steady state.** (A) Exocrine pancreas (stroma) gating strategy on live single CD45$^+$ cells and their profile based on F4/80 and CD11b surface expression (F4/80$^+$ CD11b$^+$ profile). (B) The three populations identified by F4/80$^+$ CD11b$^+$ profile (F4/80$^+$ CD11b$^+$, CD11b$^+$ F4/80$^-$, and F4/80$^-$ CD11b$^-$; from A, right) were analyzed further and highlighted in different colors (red, blue, and black, respectively). (C) The populations in B were gated on CD11c$^+$ MHC-II$^+$ for further evaluation. (D) Stromal macrophages (F4/80$^+$ CD11b$^+$, highlighted in red; left) were analyzed for expression of CD206 and CD301 (middle). Control isotype antibodies are shown on the right. Data are representative of six independent experiments. (E) Antigen presentation and T cell activation assay testing sorted macrophages (MΦ, F4/0$^+$ CD11b$^+$) from islets and the two stromal sets (CD206$^+$ and CD206$^-$). Macrophages were incubated with no antigen or titrating concentrations of either LLO peptide 190–201 or LLO protein (WW nonhemolytic variant). T cell activation was assessed by IL-2–driven [$^3$H]thymidine uptake and expressed in counts per minute (CPM). Splenic APCs were used for controls. Data presented are representative of two independent experiments performed in duplicate or triplicate. P-values were calculated using the unpaired Student's *t* test: **, P < 0.01; ***, P < 0.001; NS, P ≥ 0.05. Sample size included two to three samples per experimental group. (F) Mean fluorescent intensity (MFI) for MHC-II of stromal macrophages (CD206$^+$ and CD206$^-$). Results are pooled from three independent experiments. P-values were calculated using the Mann–Whitney *U* test: *, P < 0.05. Sample size included four independent experiments per group. Bars show the mean ± SEM.

MHC-II) and standard LLO antigen–specific T cells (Fig. 2 E; Carrero et al., 2012). Islet macrophages and stromal CD206$^-$ macrophages, which expressed relatively high amounts of MHC-II (Figs. 1 A and 2 F), stimulated T cell response to either LLO protein or peptide (Fig. 2 E). The CD206$^+$ macrophages had limited ability to present either LLO protein or peptide. This low response most likely resulted from their lower MHC-II expression (Fig. 2 F).

### Gene expression in pancreatic macrophages and modulation by diet

To assess the activation profile of the various pancreatic macrophages under steady state, islet macrophages (F4/80$^+$ CD11b$^+$) and the two sets of stromal macrophages (F4/80$^+$ CD11b$^+$ CD206$^+$ and F4/80$^+$ CD11b$^+$ CD206$^-$) were sorted by flow cytometry and evaluated by RT-PCR for canonical M1 and M2 gene expression. Islet macrophages expressed *Il1b* and *Tnfa* transcripts, whereas expression was minimal on the stromal macrophages (Fig. 3 A). *Nos2* transcripts were not detected in pancreatic macrophages. In contrast, the stromal macrophages showed an M2 profile but with differences between the two: the CD206$^+$ stromal macrophages had high expression of *Il10*, *Mrc1*, *Mgl1*, *Mgl2*, and *Fizz1*, whereas CD206$^-$ stromal macrophages expressed *Mlg1*, *Mgl2*, *Ym1*, and *Fizz1* transcripts (Fig. 3 A). The stromal macrophages both expressed *Arg1*, but at levels orders of magnitude lower than the endocrine pancreatic cells. Thus, islet macrophages were skewed to M1, whereas both subsets of stromal macrophages were skewed to M2, albeit with differences among them.

Metabolic stress is thought to skew macrophage polarization in tissues like fat (Lumeng et al., 2007; Shaul et al., 2010), specifically by favoring development of M1 macrophages that in turn promote low-level chronic inflammation (Ferrante, 2013). To asses whether metabolic stress influences changes on the activation profile of islet and stromal macrophages, 8-wk-old B6 mice were maintained either on high carbohydrate or high fat diet for five consecutive weeks. After 5 wk, mice showed a mean weight gain of ∼16% and ∼29% on high carbohydrate or high fat diet, respectively. Mice maintained on regular diet showed ∼16% weight gain. Islet and stromal macrophages on either diet (Fig. 3 B) showed the same gene expression profile as steady state untreated mice, albeit *Fizz1* had approximately six- and fourfold higher expression on stroma macrophages subsets (CD206$^+$ and CD206$^-$, respectively) when compared with steady state. In sum, the basal pancreatic macrophage activation profile was retained after metabolic stresses, but whether there are other gene expression differences besides the ones examined here needs further evaluation.

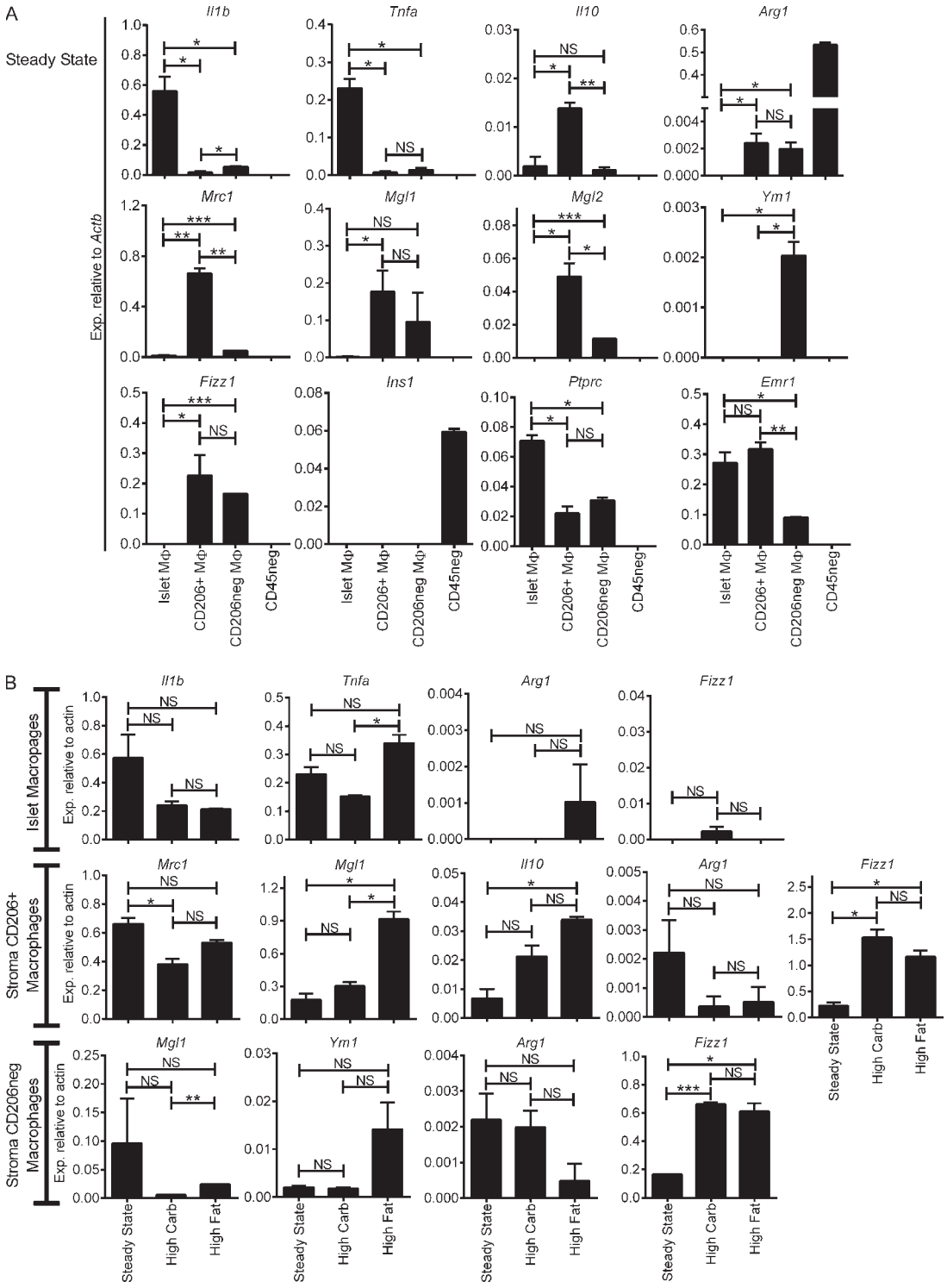


**Figure 3. Pancreatic macrophage activation profile by RT-PCR under steady state and high carbohydrate and high fat diet.** (A) Steady state islet macrophages (F4/80$^+$ CD11b$^+$) and stromal macrophages (F4/80$^+$ CD11b$^+$ CD206$^+$ and F4/80$^+$ CD11b$^+$ CD206$^-$) from 8-wk-old B6 mice were sorted and examined by qRT-PCR. CD45$^-$ (CD45neg) islet cells were used as controls for comparison. M1 (*Il1b* and *Tnfa*), M2 (*Il10*, *Arg1*, *Mrc1*, *Mgl1*, *Mgl2*, *Ym1*, and *Fizz1*), and control (*Ins1*, *Ptprc*, and *Emr1*) transcripts were assessed. Transcript expression is pooled from three independent experiments. (B) Pancreatic macrophages were maintained on high carbohydrate or high fat diet for 5 wk and assessed as in A for M1 and M2 transcripts. Comparisons of transcript expression for each pancreatic macrophage subset from two experiments are shown. All bars show the mean ± SEM. P-values were calculated using unpaired Student's *t* test: *, $P < 0.05$; **, $P < 0.01$; ***, $P < 0.001$; NS, $P \geq 0.05$. Sample size included two to three samples per experimental group.

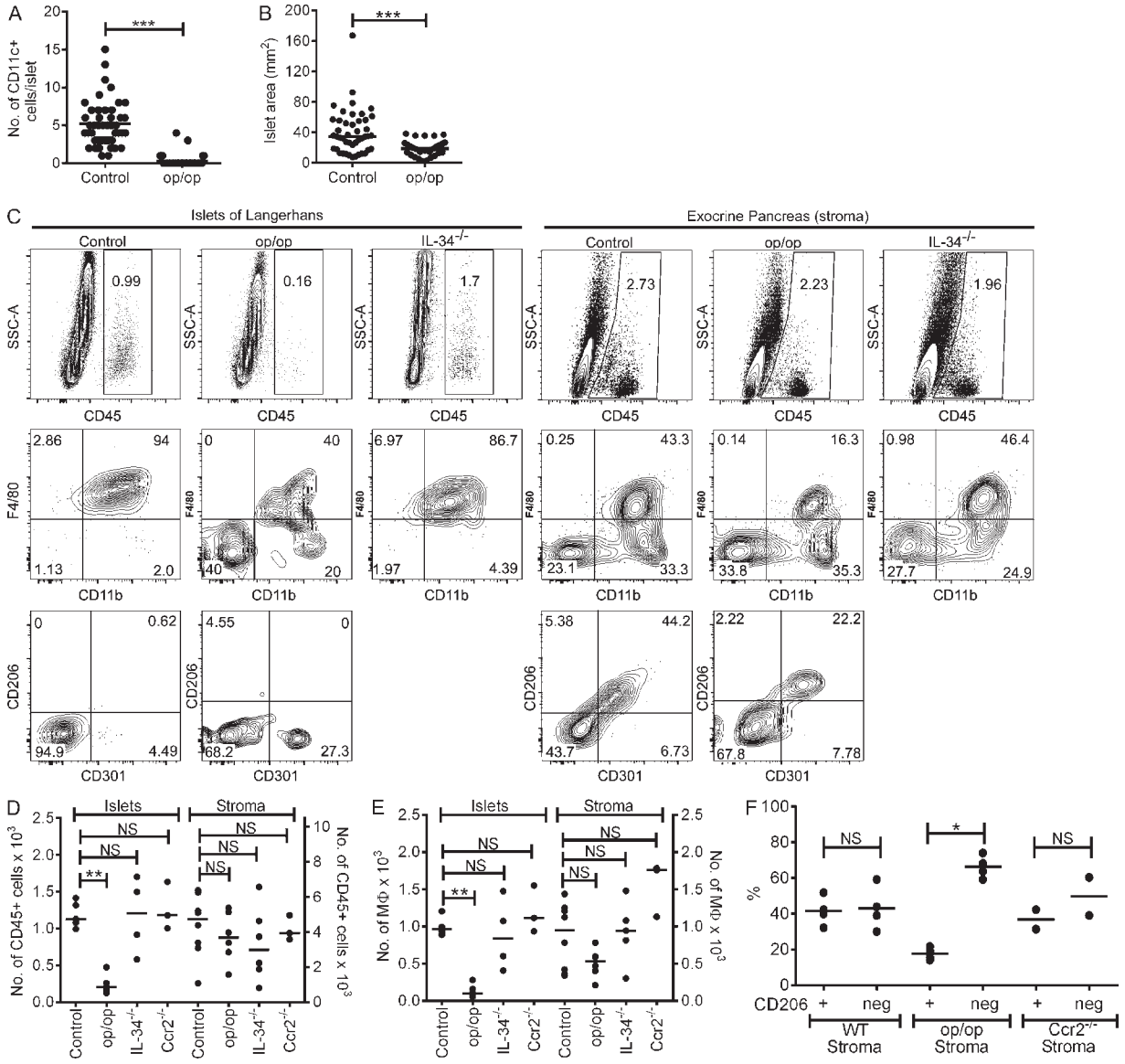


**Figure 4. Pancreatic macrophages in B6.CSF-1–deficient mice (op/op).** (A) Immunofluorescence microscopy examination of CD11c$^+$ cells in islets of WT littermates and op/op mice at 8 wk of age. Each dot represents the number of CD11c$^+$ cells per individual islet (50 examined islets per group). The experiments shown are representative of four independent evaluations. (B) Islet size was determined for islets shown in A. (C) Islets and pancreatic stroma from 8-wk-old WT littermates (Control) and op/op and IL-34$^{-/-}$ mice analyzed by flow cytometry. Islets and stroma were gated on singlets for CD45$^+$ (top) and plotted for F4/80 and CD11b (middle) and for CD206 and CD301 (bottom). (D and E) Quantitative absolute numbers from pooled independent experiments showing total CD45$^+$ cells (D) and macrophages (gated on F4/80$^+$ CD11b$^+$; E) in islets and stroma of control, op/op, IL-34$^{-/-}$, and Ccr2$^{-/-}$ mice. (F) Percentages of stromal CD206$^+$ and CD206$^-$ macrophages from independent experiments in control, op/op, and Ccr2$^{-/-}$ mouse strains. All scatter plots show bars that represent mean values. P-values were calculated using the Mann–Whitney *U* test: *, P < 0.05; **, P < 0.01; ***, P < 0.001; NS, P ≥ 0.05.

### Pancreatic macrophage dependency on CSF-1

Mice lacking functional CSF1 (op/op) show developmental alterations in many organs and absence of macrophages in several tissues, reinforcing the role for macrophages in tissue development and homeostasis (Pollard et al., 1997; Banaei-Bouchareb et al., 2004). The islets of op/op mice were small (Pollard et al., 1997) and had a reduction in the mean number of macrophages (Calderon et al., 2008). Fig. 4 A shows by direct microscopy that ∼85% of the islets from op/op mice lacked macrophages, whereas the remaining ∼15% contained one to four per islet. The islet mean area comparison between control littermates and op/op mice was found to be ∼40 mm$^2$ and ∼20 mm$^2$, respectively, indicating a reduced islet size in the op/op mice (Fig. 4 B). Flow cytometry analysis of op/op islets showed ∼85% reduction in the number of islet leukocytes and statistical difference by absolute numbers (Fig. 4, C–E).

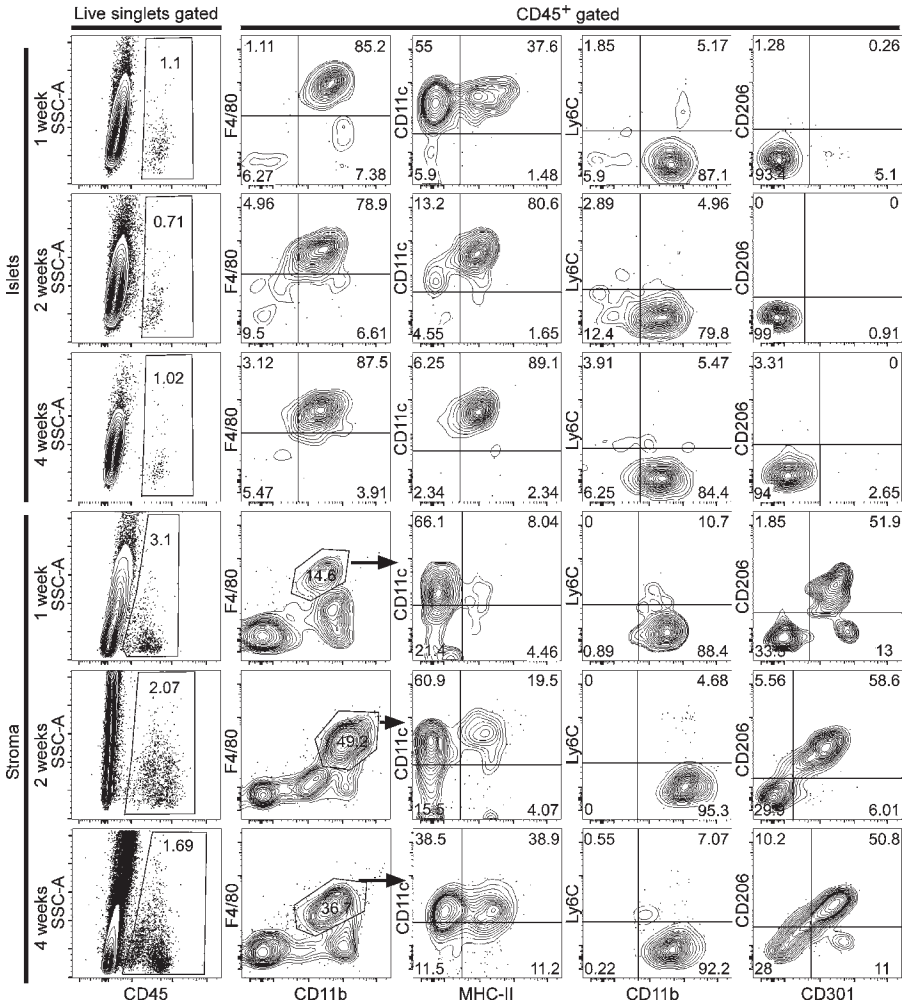


**Figure 5. Pancreatic macrophages in early postnatal life.** Islets and stromal macrophages from 1-, 2-, and 4-wk-old mice (gated on live singlets for CD45+) were evaluated for expression of F4/80, CD11b, CD11c, MHC-II, Ly6C, CD206, and CD301. Islet macrophages were gated from all CD45+ islet cells, whereas pancreatic stroma macrophages were gated on F4/80+ CD11b+ profile (indicated by arrows). Data are representative of two independent experiments at 1 wk and three independent experiments at 2 and 4 wk, each having four to eight mice per time point.

Of the remaining islet leukocytes in the op/op mouse, ∼40% showed a macrophage profile (F4/80$^+$ CD11b$^+$), ∼20% showed F4/80$^-$ CD11b$^+$, and the remaining cells (∼40%) lacked both (Fig. 4 C). The F4/80$^-$ CD11b$^-$ cells also lacked CD11c, MHC-II, Ly6C, CD8α, Siglec-H, CD103, B220, CD19, and CD3ε. They may represent an early macrophage precursor.

In contrast to the reduction in islet macrophages in the op/op mice, the pancreatic stromal macrophages were less affected (Fig. 4, C–E). Although the CD206$^+$ and CD206$^-$ macrophages were equally distributed in the B6 mouse, there was a selective loss of the CD206$^+$ macrophages in the op/op mice, but the CD206$^-$ were at WT numbers (Fig. 4 F). To assess whether pancreatic stromal macrophages were dependent on another ligand for their CSFR1, we evaluated IL-34$^{-/-}$ mice (Lin et al., 2008; Wang et al., 2012). IL-34$^{-/-}$ mice showed no alteration of pancreatic macrophages (Fig. 4, C–E).

### Pancreatic macrophage maintenance is CCR2 independent

We also examined B6.CCR2$^{-/-}$ mice that have a reduction of Ly6C$^{hi}$ circulating monocytes (Serbina and Pamer, 2006). B6.CCR2$^{-/-}$ mice showed no difference in islets and stromal macrophage (Fig. 4, D and E). Stromal macrophages contained equal percentages of the two macrophage subsets (CD206$^+$ CD301$^+$ and CD206$^-$ CD301$^-$; Fig. 4 F). In brief, the maintenance of islet and pancreatic stromal macrophages was CCR2 independent.

### Pancreatic macrophages at various times after birth

To address when macrophages can be found in the islets and pancreatic stroma after birth as well as their initial profile, we isolated islets at 1, 2, and 4 wk of age. Islet macrophages (F4/80$^+$ CD11b$^+$) were found at 1 wk after birth and were negative for CD206 and CD301, but their expression of MHC-II molecules was limited to ∼35% of the population (Fig. 5). At 2 wk of age, islet macrophage expression for MHC-II was found to be ∼80%. By 4 wk of age, islet macrophages resembled the adult profile (F4/80$^+$ CD11b$^+$ MHC-II$^+$). Attempts to isolate pure islets for flow cytometric assessment of resident macrophages before 1 wk of age were not reliable. A previous study identified macrophages embedded within the early islet cluster formation on pancreatic sections at embryonic day (E) 17.5 (Geutskens et al., 2005). Pancreatic stroma macrophages were identified but reduced in percentage

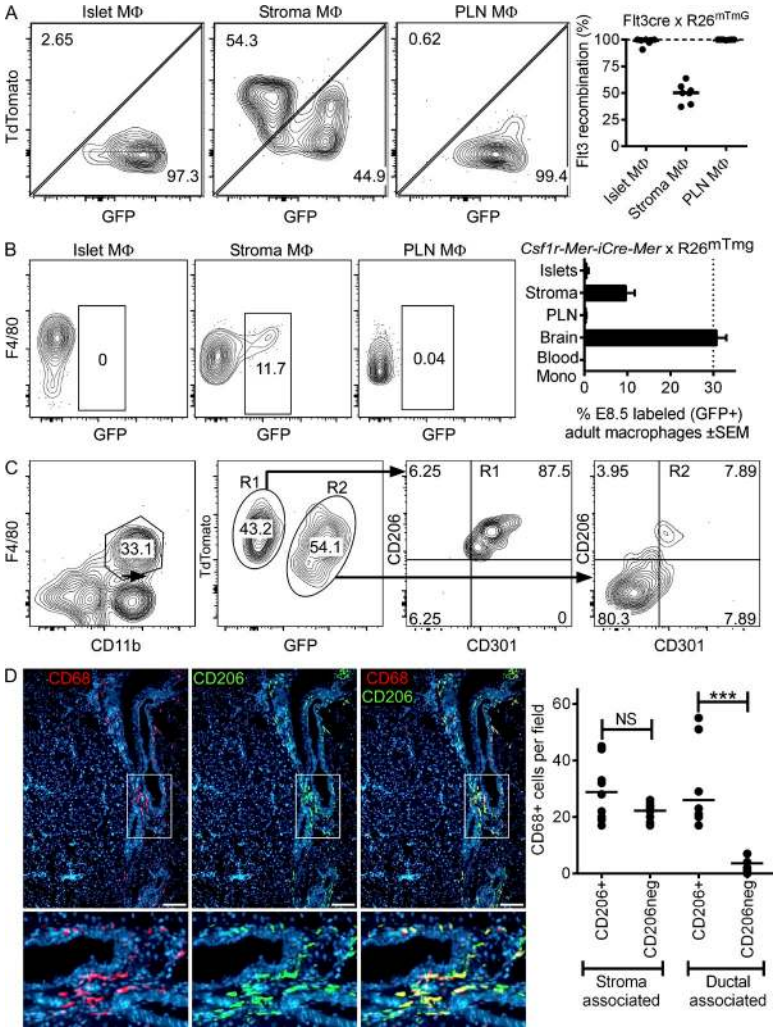


**Figure 6. Ontogeny of pancreatic macrophages.** (A) *Flt3-cre* × *Rosa*$^{mTmG}$ reporter mice (13–14 wk of age) were analyzed by flow cytometry and gated on singlets for CD45$^+$ cells and macrophages (F4/80$^+$ CD11b$^+$) from islets, stroma, and PLNs to evaluate GFP and tdTomato (TdTom$^+$) expression. Pooled results (right) from seven independent evaluations are shown. (B) *Csf1r-Mer-iCre-Mer* × *Rosa*$^{mTmG}$ reporter mice were gavaged with tamoxifen at E8.5 to label the progeny of yolk sac macrophages (TdTomato$^-$ GFP$^+$). Islets, stroma, and PLN macrophages were evaluated at 10 wk of age to determine whether yolk sac progeny persisted into adulthood. Pooled results (right) from two experiments show the percentage of labeled (GFP$^+$) macrophages (islets, stroma, and PLNs), brain microglia, and blood monocytes. Bars indicate the mean ± SEM. (C) Pancreatic stroma of *Flt3-cre* × *Rosa*$^{mTmG}$ reporter mice (13–14 wk of age) were analyzed by flow cytometry and gated on macrophages (F4/80$^+$ CD11b$^+$) for their TdTom$^+$ or GFP$^+$ expression (R1 and R2 gates, respectively) to evaluate CD206 and CD301 profiles. Data are representative of two independent experiments. (D) Immunofluorescence examination of pancreatic sections from 10-wk-old mice showing stromal macrophage distribution (stained for CD68 in red), their positive or negative expression for CD206 (green), and nuclear staining by DAPI (blue). Higher magnifications of the periductal area (boxes) are shown below. Images are representative of 8–10 sections from two examined mice. Bars, 100 µm. (right) Quantitative analysis showing distribution of CD206$^+$ and CD206$^-$ macrophages in stroma and ductal-associated areas. Bars indicate the mean. P-values were calculated using the Mann–Whitney *U* test: ***, $P < 0.001$; NS, $P \geq 0.05$.

at 1 wk of age (∼15%), contained limited expression of MHC-II molecules (∼8%), and showed the two macrophage sets (CD206$^+$ CD301$^+$ and CD206$^-$ CD301$^-$) in equal percentages (Fig. 5). At 2 wk of age, the stroma macrophage represented ∼50% of the leukocytes, ∼20% expressed MHC-II, and contained the two subsets (CD206$^+$ CD301$^+$ and CD206$^-$ CD301$^-$). By 4 wk of age, stromal macrophages showed similar membrane expression (F4/80, CD11b, and MHC-II) as adult stromal macrophages.

### Embryological sources of pancreatic macrophages

We examined the embryonic derivation of the pancreatic macrophages. Embryonic-derived macrophages are generated in two stages. The initial source is during embryonic development by primitive hematopoiesis (E7.5–11.5) found in the yolk sac, where progenitors give rise to macrophages and red blood cells (Lichanska et al., 1999; Lichanska and Hume, 2000; Kumaravelu et al., 2002; Epelman et al., 2014a). The second source is from definitive hematopoiesis that develops in the fetal liver (E11.5–16.5), generating monocyte-derived macrophages. Postnatally, fetal liver hematopoiesis is replaced by BM hematopoiesis, which becomes the source of circulating monocytes. The identification of primitive hematopoiesis-derived macrophages in the pancreas was previously reported by Schulz et al. (2012). However, the study did not identify their anatomical location.

To determine the origin of islet-resident macrophages in the adult pancreas, we evaluated the *Flt3-cre* × *Rosa*$^{mTmG}$ mouse (Boyer et al., 2011, 2012). This reporter mouse allows the identification of definitive hematopoiesis (adult hematopoietic stem cell [HSC] derived) by the transient up-regulation of FLT3 in all definitive HSCs as they separate into different lineages (Böiers et al., 2010; Buza-Vidas et al., 2011). This reporter mouse has constitutive expression of TdTomato in all cells. Upon *Flt3-cre* expression, cells turn off TdTomato expression and express GFP. This system parses macrophages into two developmental origins: TdTomato$^-$ GFP$^+$ (FLT3-Cre$^+$) macrophages are definitive hematopoiesis derived (adult HSC derived) and TdTomato$^+$ GFP$^-$ (FLT3-Cre$^-$) macrophages are embryonic lineage derived (yolk sac or fetal monocyte derived; Fig. S3 A; Schulz et al., 2012; Epelman et al., 2014b).

We analyzed the F4/80$^+$ CD11b$^+$ leukocytes in islets, pancreatic stroma, and pancreatic LNs (PLNs) of the *Flt3-cre* × *Rosa*$^{mTmG}$ reporter mice at 13–14 wk of age. Recombination rates driven by *Flt3-cre* ranged from 82 to 98% in blood monocytes at the time of observation. All islet macrophages were TdTomato$^-$ GFP$^+$, indicating them to be adult HSC derived (Fig. 6 A). The stromal macrophages contained two populations (TdTomato$^-$ GFP$^+$ and TdTomato$^+$ GFP$^-$), the first being adult HSC derived, whereas the latter may represent macrophages established by any of two embryonic lineages (yolk sac derived and/or fetal monocyte derived; Fig. 6 A).

To assess whether the contribution of stromal GFP-negative macrophages identified in the *Flt3-cre* × *Rosa*$^{mTmG}$ reporter mouse model derived from yolk sac or fetal monocytes, we used the *Csf1r-Mer-iCre-Mer* × *Rosa*$^{mTmG}$ mouse model. This model labels yolk sac–derived macrophages (TdTomato$^-$ GFP$^+$) by the administration of tamoxifen at E8.5 (Fig. S3 B; Schulz et al., 2012; Epelman et al., 2014a). The labeling efficiency of macrophages at E10.5 was found to be 40%. The presence of yolk sac–labeled macrophages was evaluated in the pancreas at 10 wk of age. Islet-resident macrophages showed only the presence of TdTomato$^+$ GFP$^-$ (Fig. 6 B), indicating them not to be yolk sac derived and in agreement with the *Flt3-cre* mouse model results. Stromal macrophages showed the presence of ∼10% TdTomato$^-$ GFP$^+$, indicating the contribution of yolk sac–derived macrophages in the pancreatic stroma.

We conclude that from the 54% stromal macrophages that were not HSC derived (Fig. 6 A), about half originated from yolk sac, primitive hematopoiesis, whereas the rest were of undetermined origin but likely derived from fetal liver monocytes. From a previous published study using these same mice, adult brain microglia remained labeled at ∼30% (Epelman et al., 2014a), indicating that yolk sac–derived macrophages labeled at E8.5 persisted at 10 wk of age (Fig. 6 B).

Interestingly, in the *Flt3-cre* × *Rosa*$^{mTmG}$ reporter mouse model the TdTomato$^+$ GFP$^-$ stromal macrophages (yolk sac derived and/or fetal monocyte derived) expressed both CD206 and CD301, whereas the adult HSC–derived stromal macrophages (TdTomato$^-$ GFP$^+$) did not (Fig. 6 C). Further evaluation for the distribution of CD206$^+$ and CD206$^-$ macrophages on pancreatic sections identified a preferential localization of the CD206$^+$ subset to the periductal area (Fig. 6 D). In sum, the pancreas has macrophages from different lineages in distinct anatomical sites: the islet macrophages derive from adult HSCs and have an M1 profile; the stromal macrophages have two distinct origins, yet both sets have an M2 gene expression profile.

### Replacement and proliferation rates among pancreatic macrophages

To examine the turnover rates of islet and stromal macrophage, CD45.1$^+$ and CD45.2$^+$ mice were joined in parabiosis. After 6 wk, islets and stroma were examined for the presence of CD45.1$^+$ or CD45.2$^+$ cells in each partner. Blood Ly6C$^{hi}$ monocyte chimerism was ∼30%. The percentage of blood chimerism was used to normalize percentages of nonhost-derived macrophages. Replacement of islet macrophages by nonhost-derived monocytes was marginal (median of 4.8% from the three independent experiments), indicating that most are long lived with minimal contribution by circulating monocytes (Fig. 7 A). The same findings were made with the CD206$^+$ CD301$^+$ stromal macrophages (Fig. 7 A, middle and bottom). In contrast, CD206$^-$ CD301$^-$ stromal macrophages showed a median of 28.9% chimerism (Fig. 7 A, middle and bottom). In sum, the only macrophage set that had a continual exchange with circulating blood cells was the CD206$^-$ CD301$^-$ stromal set.

To assess the extent of in situ macrophage proliferation, islets and stroma were examined at three different time points of BrdU administration. BrdU incorporation by macrophages was not detected after pulses of 2 or 24 h. In contrast, after 7 d of ad libitum BrdU exposure, islet and stromal macrophages were ∼20–50% BrdU$^+$ (Fig. 7, B and C). Lower numbers of BrdU$^+$ cells were identified in islet and CD206$^+$ stroma macrophages. In accordance with their exchange by circulating blood cells shown in the parabiosis results, the CD206$^-$ stroma macrophages had a higher amount of BrdU incorporation (Fig. 7, B and C). PLN macrophage BrdU incorporation was ∼50% after a 7-d pulse. BM BrdU incorporation at this time point was found to be >95% (Fig. 7, B and C). Together, these data support the hypothesis that resident macrophages have a long half-life and are self-maintained by in situ proliferation.

### Pancreatic macrophages after genotoxic insult

Most tissue-resident macrophages (with the exception of the microglia) can be replaced by BM-derived precursors after lethal irradiation (Haniffa et al., 2009; Ginhoux et al., 2010; Ajami et al., 2011; Hashimoto et al., 2013; Lavin et al., 2014). We evaluated whether there was replacement of islet and stromal macrophages by donor-derived CD45.1 BM cells transplanted into lethally irradiated B6 CD45.2 mice. After 2 wk of transplantation, donor-derived myeloid cells represented ∼35% of the CD45$^+$ cells in the islets (Fig. 8 A). Of these, half showed an islet-resident macrophage profile (F4/80$^+$ CD11b$^+$ Ly6C$^-$), whereas the remaining showed a monocyte profile (CD11b$^+$ F4/80$^{low}$ Ly6C$^-$ and CD11b$^+$ F4/80$^{low}$ Ly6C$^+$). By 3 wk, donor-derived islet macrophages (CD45.1$^+$) represented ∼78% of the total islet myeloid composition with few monocytes present. At 7 and 15 wk, donor-derived islet macrophages had completely replaced the host macrophages (∼93 and ∼100%, respectively; Fig. 8 A) and displayed the steady state M1 profile, including expression of *Il1b* and *Tnfa* (Fig. 9 C).

Stromal macrophage replacement after genotoxic insult showed similar kinetics of replacement as the islet macrophages. At 3 and 7 wk after transplantation, ∼80% of stroma macrophages (F4/80$^+$ CD11b$^+$) were donor derived (CD45.1$^+$), from which ∼40% expressed Ly6C (Fig. 8 B). By 15 wk, donor-derived macrophages had completely replaced the host macrophages (∼98%) and Ly6C expression was minimal, indicating a steady state macrophage profile (Fig. 8 B). 9 wk after transplant, the donor-derived stromal macrophages

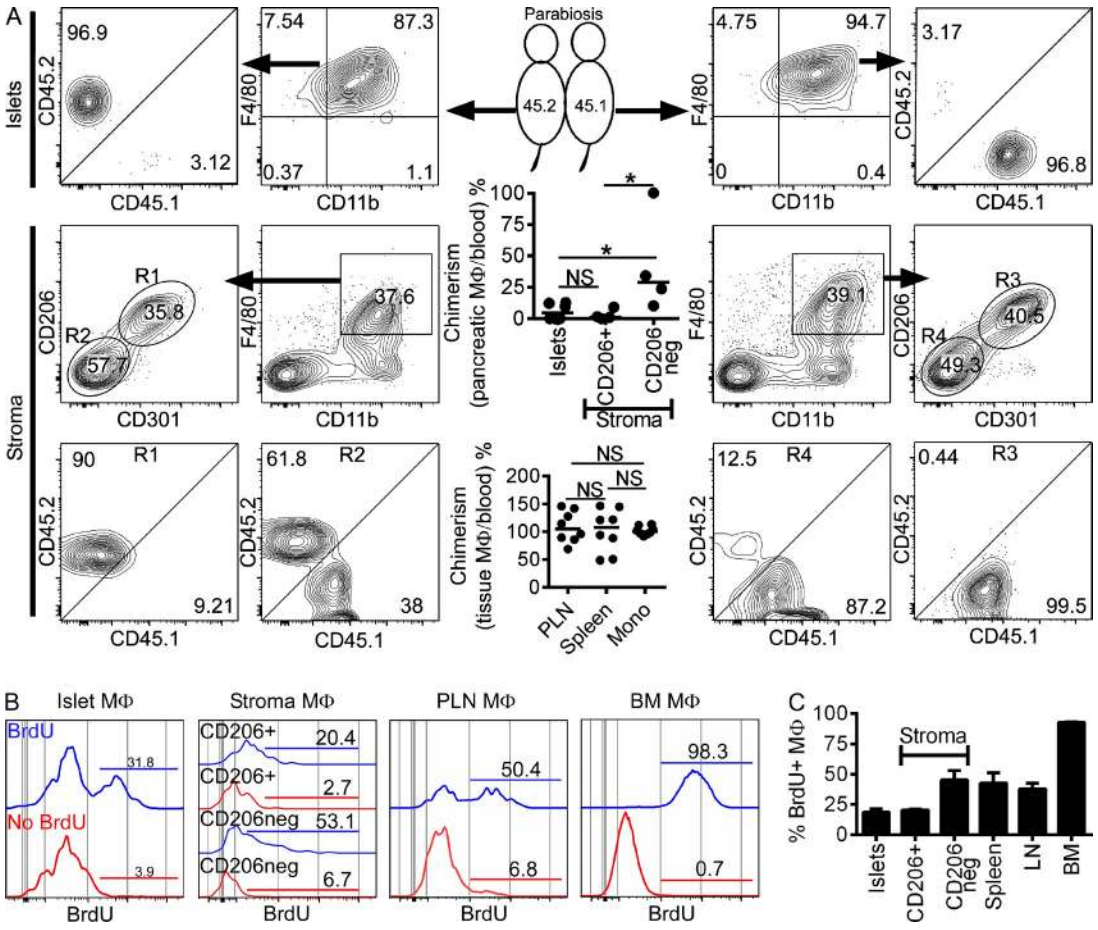


**Figure 7. Pancreatic macrophages after parabiosis and in situ maintenance.** (A) Parabiotically joined CD45.2$^+$ (left) and congenic CD45.1$^+$ mice (right) were examined at 6 wk of parabiosis. Islets and stroma macrophages (gated on F4/80$^+$ CD11b$^+$, and CD206$^+$ CD301$^+$ or CD206$^-$ CD301$^-$ expression [R1 and R2 gates, respectively]: middle and bottom) along with their CD45.1$^+$ or CD45.2$^+$ expression are shown. The top scatter dot plot panel shows pooled quantitative pancreatic macrophage chimerism percentages at 6 wk of parabiosis for islet chimerism (total of 12 mice from three independent experiments, pooling 2 mice per parabiont side) and stromal CD206$^+$ and CD206$^-$ macrophages (from two independent experiments using single parabionts). The bottom scatter dot plot panel shows pooled quantitative tissue macrophage chimerism percentages (PLNs and spleen) from the same experiments and compared with blood monocyte chimerism for each parabiont. Bars represent mean values. (B) Islet, pancreatic stroma (CD206$^+$ and CD206$^-$), PLN, and BM macrophage (MΦ) proliferation was assessed after 7 d of ad libitum BrdU treatment. Histograms of macrophages (gated on CD45$^+$; F4/80$^+$ and CD11b$^+$) with or without BrdU treatment (blue and red histogram lines, respectively) are shown. Bars indicate percentages of BrdU incorporation. (C) Pooled results for BrdU incorporation as shown in B from three independent experiments. Bars indicate the mean ± SEM. P-values were calculated using the Mann–Whitney *U* test: *, $P < 0.05$; NS, $P \geq 0.05$.

divided into two subsets (CD206$^+$ CD301$^+$ and CD206$^-$ CD301$^-$), which corresponded to the two stromal macrophage subsets under steady state (Fig. 9, A and B). Both donor-derived stromal macrophage subsets maintained an M2 profile, as seen under steady state (CD206$^+$ macrophages had high expression of *Il10* and *Fizz1*, whereas CD206$^-$ macrophages expressed *Ym1* and *Fizz1* transcripts; Fig. 9 C).

In conclusion, myeloablation by γ-irradiation allowed the entry of donor-derived myeloid cells that then differentiated into resident macrophages. Islet and stromal macrophages differentiated and maintained a similar activation profile as seen under steady state, suggesting that each tissue region (endocrine or exocrine component of the pancreas) modulated the properties of the macrophage lineage.

## DISCUSSION

Each tissue conditions the physiology of the macrophages and sets up a potentially symbiotic relationship between their resident cells and the macrophages. Our study adds the pancreas to the series of studies examining the macrophage populations of different organs and documents the plasticity of this lineage (Murray and Wynn, 2011; Epelman et al., 2014b; Murray et al., 2014). Although several studies have evaluated pancreatic macrophages (Hume et al., 1984; Banaei-Bouchareb et al., 2004; Geutskens et al., 2005; Ehses et al., 2007; Calderon et al., 2008, 2014; Melli et al., 2009; Mohan et al., 2010; Yin et al., 2011; Cucak et al., 2014; Ferris et al., 2014; Ino et al., 2014; Westwell-Roper et al., 2014; Xiao et al., 2014), this is the first study to examine their origin, turnover, and functional features

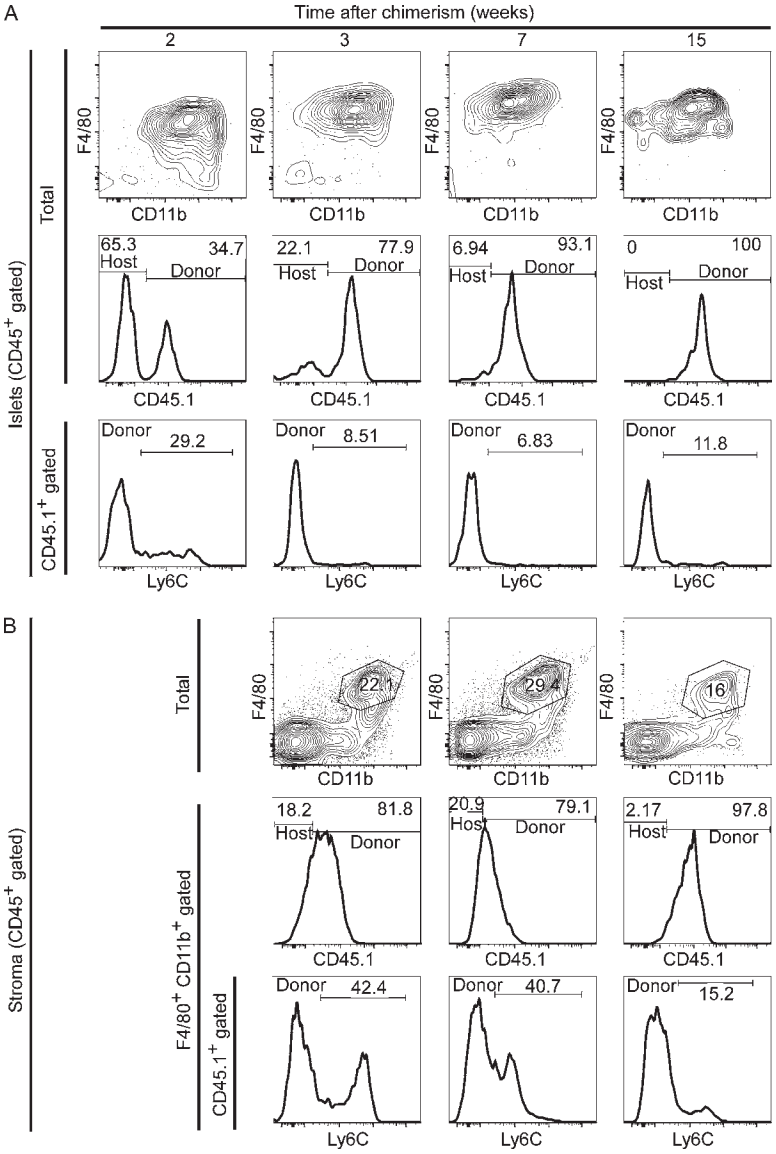


**Figure 8. Replacement of pancreatic macrophages after genotoxic insult.** Lethally irradiated CD45.2 B6 mice received CD45.1 congenic B6 BM transplant. (A and B) CD45+ gated islet cells (A) and pancreatic stroma cells (B) were examined at different chimerism time points. (A, top) CD45+ cells showing F4/80 and CD11b profile. (middle) CD45+ cells evaluated for the presence of CD45.1+ (donor) and CD45.1− (host). (bottom) Histograms of CD45.1+ gated cells (donor) for Ly6C expression. (B, top) CD45+ cells showing F4/80 and CD11b profile. (middle) F4/80+ CD11b+ gated cells evaluated for CD45.1+ (donor) and CD45.1− (hosts) expression. (bottom) Histograms of CD45.1+ F4/80+ CD11b+ gated cells (donor macrophages) for Ly6C expression. Data are a representative of three independent experiments.

at both the exocrine and endocrine sites under noninflammatory conditions (steady state).

The pancreas was notable for the differences between the macrophages residing in the interacinar stroma and those within the islets of Langerhans. Both sites contained long-lived cells that interchanged to a minimum with blood monocytes, an issue that was made very clear in the parabiosis experiments. Also, both were affected, albeit to variable degree, by CSF1 deficiency. The major distinguishing features concerned their origin, expression profiles, and turnover. As first recorded by Schulz et al. (2012), about half of the pancreatic macrophages are derived from primitive hematopoiesis. Our studies pinpoint the novel feature that these set of macrophages reside exclusively in the stroma, whereas those in the islets are entirely derived from definitive hematopoiesis (adult HSC derived; Fig. S4).

A second important difference between the two sets of macrophages concerned their functional characteristics. Macrophages in islets under steady state had features of activation, including high expression of class II MHC molecules, effective antigen presentation to T cells, and also having an M1-like activation profile (*Il1b* and *Tnfa* transcripts). In contrast to the islets, the macrophages of the acinar stroma showed a M2 polarization and were composed of two subsets, one being high on MHC-II expression and antigen presentation, whereas the second showed low MHC-II, limited antigen presentation, and preferential localization to the periductal area. The function of these sets of macrophages is not apparent, whether they regulate angiogenesis or lymphogenesis is one speculation. To be noted is that the functional features were not noticeably changed by high fat or carbohydrate diet. These resident stromal macrophages could be involved in the fibrogenesis that accompanies ductal adenocarcinoma (Chu et al., 2007; Clark et al., 2007). One study showed the presence of M2-like macrophages involved in the regeneration of

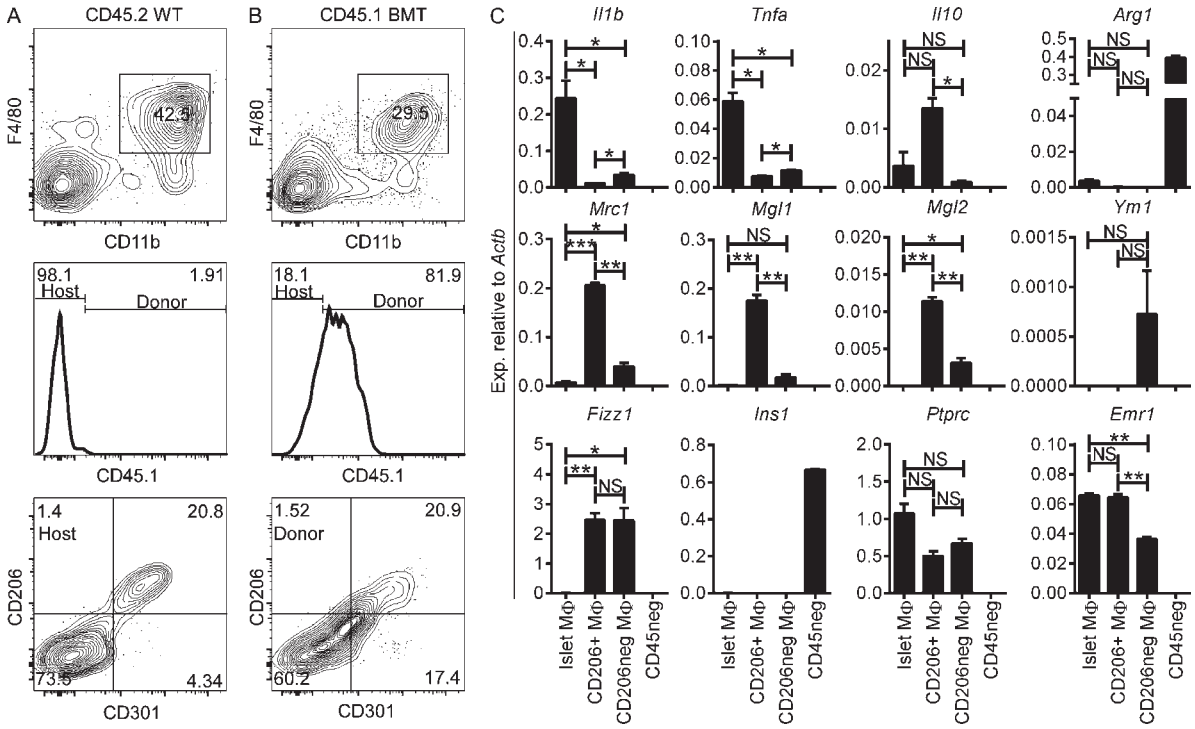


**Figure 9. Pancreatic macrophage profiles after genotoxic insult.** (A and B) Stroma from WT CD45.2 (A) and CD45.2 mice receiving CD45.1 BMT (CD45.1 BMT; B) after genotoxic insult and evaluated at 9 wk after transplant. (top) Stroma cells (gated on singlets CD45$^+$) showing F4/80 and CD11b profile. (middle) Histograms of F4/80$^+$ CD11b$^+$ gated cells (from top panels) evaluated for the presence of CD45.1$^+$ (donor) and CD45.1$^-$ (host) macrophages. (bottom) Histograms of F4/80$^+$ CD11b$^+$ gated cells from CD45.2 WT and CD45.1 BMT showing CD206 and CD301 expression. Data are a representative of two independent experiments. (C) Sorted islet macrophages (CD45$^+$ F4/80$^+$ CD11b$^+$) and stromal macrophages (CD45$^+$ F4/80$^+$ CD11b$^+$ CD206$^+$ and CD45$^+$ F4/80$^+$ CD11b$^+$ CD206$^-$) from CD45.2 WT and CD45.1 BMT mice at 9 wk after transplant. CD45-negative (CD45neg) islet cells were used as controls for comparison. M1-like (*Il1b* and *Tnfa*), M2-like (*Il10*, *Arg1*, *Mrc1*, *Mgl1*, *Mgl2*, *Ym1*, and *Fizz1*), and control (*Ins1*, *Ptprc*, and *Emr1*) transcripts were assessed. Transcript expression is pooled from two independent experiments performed in duplicate. Bars represent the mean ± SEM. P-values were calculated using the unpaired Student's *t* test: *, P < 0.05; **, P < 0.01; ***, P < 0.001; NS, P ≥ 0.05. Sample size included two samples per experimental group.

the pancreas after pancreatic duct ligation, but there was no untreated stromal macrophage evaluation (Xiao et al., 2014).

Turnover rates of the resident macrophages vary greatly in the degree of replacement by monocytes (Ginhoux et al., 2010; Hoeffel et al., 2012; Guilliams et al., 2013; Hashimoto et al., 2013; Yona et al., 2013; Bain et al., 2014; Epelman et al., 2014a,b; Molawi et al., 2014). The islet macrophage was long lived, not replaceable by blood monocytes under steady state, self-replicating, and was displaceable only after lethal irradiation. To add to the issue of the plasticity of the lineage, although the primitive hematopoiesis-derived stromal macrophages were M2, expressed CD206/CD301, and were long lived, the stromal set derived from definitive hematopoiesis were also M2 but lacked the CD206/CD301 markers and were replaceable by blood monocytes. Thus, it appears that the stromal milieu sets the response of the macrophages.

Our laboratory has paid much attention to the resident islet phagocytes in the context of our interest in examining the presentation of diabetogenic antigens. A recent study in the diabetic-prone NOD mouse established the presence of the islet macrophages together with a small set of CD103$^+$ DCs under the control of the *Batf3* transcription factor; the latter were essential for the initiation of the autoimmune process (Ferris et al., 2014). The CD103$^+$ DC is not found in the B6 mouse strain, suggesting that its presence is not homeostatic, but pathogenic in the context of the islet. The islet macrophages captured diabetic antigens, were always next to blood vessels, and protruded cytoplasmic extensions into their lumen (Calderon et al., 2008, 2014). As shown now, these are long lived cells and have an islet support function very evident in the op/op mouse. The presentation of diabetic antigens by islet macrophages is not strictly linked to the NOD. In B10.BR mice we also showed that they contained antigens from β cells and could present them to T cells (Calderon et al., 2008). It remains unknown whether the earliest diabetogenic APC in the islet that primes T cells is the macrophage and/or the CD103$^+$ DC, which is an area of current investigation.

Islet macrophages have also been discussed in the context of the metabolic changes taking place in type 2 diabetes (Ehses et al., 2007; Richardson et al., 2009; Westwell-Roper et al., 2014). In the limited analysis made here, macrophages

from mice fed a high carbohydrate or high fat diet had the same functional features in the sense of an M1 polarization in islets but maintained the M2 features in the stroma. This finding is different from the macrophages of adipose tissue that change from their basal M2 profile to an M1 in obese mice (Lumeng et al., 2007; Shaul et al., 2010).

As in other tissues, the resident macrophages were replaced by BM cells under myeloablative procedures. This allowed us to examine how the new macrophages were differentiating in the two anatomical sites. We showed the same biochemical features from their basal state, i.e., M1 in islets and M2 in the stroma. We are unsure how the distinction between stromal and islet macrophages is established. Several potentially overlapping events may be taking place that need to be determined. Is it possible that the earliest macrophage precursors are precommitted to a particular role (M1/M2, supportive, or immune protective, etc.) and that the local microenvironment provides the recruiting and retention signals specific for the needed cell type? Alternatively, is the nascent macrophage a truly "blank-slate" or in a so-called "M0" condition and able to turn on gene expression networks suitable for the environment it senses? For example, the high proteolytic and bicarbonate-rich environment of the stroma could be sensed as a distinct environment from the hormone-rich environment of the islets of Langerhans and lead to functional specialization that allows the macrophage to support the different cells present in these environments (Gosselin et al., 2014; Lavin et al., 2014). Finally, can this phenotypic profile be influenced by drugs to intervene in the many diseases that are linked to macrophage function/dysfunction?

Future studies should aim to examine how each anatomical site conditions the two sets of resident macrophages in the pancreas. It is likely that the paradigm of location-specific macrophage pools that we uncover in the pancreas can be extended to other organs. Most organs are known to contain more than one resident macrophage phenotype. The diversity of splenic macrophage phenotypes with respect to location is well appreciated but poorly understood or explored. Distinct resident macrophages have been demonstrated in the lung, peritoneum, and heart (Hashimoto et al., 2013; Yona et al., 2013; Epelman et al., 2014a). In these organs, minimal evaluation has been performed on the possibility that the distinct phenotypes are driven by distinct macrophage localization within the organ. In brief, in the last few years, macrophage biologists have come to appreciate the diversity of these subsets within different organs. Our findings push this consideration further by highlighting the crucial need to consider intraorgan anatomy as the field moves into the future.

## MATERIALS AND METHODS

**Mice.** B6 mice were obtained from the National Cancer Institute and bred in our facility. B6.Zbtb46$^{GFP/+}$ and B6.Notch2$^{f/f}$ CD11c-cre mice were provided by K.M. Murphy (Satpathy et al., 2012, 2013). B6.CX$_3$CR1$^{GFP/+}$ and B6.LyzM$^{GFP/+}$ mice were provided by G.J. Randolph. B6.*Flt3-cre* × *Rosa*$^{mTmG}$ and B.6.*Csf1r-Mer-iCre-Mer* × *Rosa*$^{mTmG}$ mice were provided by S. Epelman (Boyer et al., 2011; Epelman et al., 2014a). *Csf1r-Mer-iCre-Mer* × *Rosa*$^{mTmG}$ pregnant mice received 2 mg tamoxifen gavaged in 100 µl corn oil at E8.5 to label yolk sac macrophages (Schulz et al., 2012). B6.CCR2$^{-/-}$ mice were provided by W.M. Yokoyama. B6.IL-34$^{-/-}$ mice were provided by M. Colonna (Washington University in St. Louis; Wang et al., 2012). B6.CSF1-deficient mice (B6;C3Fe a/a-Csf1$^{op}$/J; op/op) and B6-Ly5.1 (CD45.1) were obtained from the Jackson Laboratory. All experiments were approved by the Division of Comparative Medicine of Washington University School of Medicine in St. Louis (Association for Assessment and Accreditation of Laboratory Animal Care, accreditation number A3381-01). CD45.2 and CD45.1 B6 female mice controlled for age and weight were parabiosed by matching longitudinal skin incisions on the flanks. Their elbows and knees were then joined with dissolvable sutures, and the incisions were closed with wound clips. Postoperative care included administration of Buprenex compound for pain management, 5% dextrose, and 0.9% sodium chloride. Nutritional gel packs were provided in each cage and antibiotics (Sulfatrim) in the drinking water for the duration of the experiment (Peng et al., 2013; Sojka et al., 2014). For BM transplantation experiments, CD45.2 B6 mice were irradiated (950 cGy, two split doses, 5 h apart) and were given 5 × 10$^6$ total BM cells from CD45.1 B6 mice. For experimental mice on high carbohydrate or high fat diet, 8-wk-old female B6 mice were maintained for 5 wk on 70% carbohydrate with adjusted vitamins or 60% fat adjusted chow (Teklad; Harlan Laboratories, Inc.) and followed for weight gain weekly.

**Histology.** B6 pancreata were frozen and embedded in Tissue-Tek (Sakura). Tissue sections were stained for 1 h at room temperature with Alexa Fluor 647 anti-CD68 (FA-11) and Alexa Fluor 488 anti-CD206 (C068C2; BioLegend) using CAS-Block Histochemical Reagent (Life Technologies) as the diluent and finally washed three times in PBS for 5 min each. DAPI mounting medium (Vector Laboratories) was used for nuclear staining. Microscopy imaging was performed using an Eclipse E800 microscope (Nikon) equipped with CFI Plan Apo Lambda DM 20× air objective, EXFO X-Cite 120PC light source (EXFO), EXi blue fluorescence microscopy camera, and QCapture 64-bit v2.9.13 acquisition software (QImaging).

**Islets and pancreatic stroma isolation.** Pancreata were perfused through the common bile duct (5 ml HBSS without calcium supplemented with collagenase), removed, and digested in a 37°C water bath for 15 min. After shaking for 90 s, pancreata were washed three times and passed through a 70-µm cell strainer to retain the islets (Salvalaggio et al., 2002; Li et al., 2009). The content passed through the 70-µm cell strainer represented the pancreatic stroma. Islets retained on the cell strainer were flushed from the filter onto a Petri dish for hand-picking using a zinc-chelating dye (Dithizone; Sigma-Aldrich; 200 µg/ml of 10% DMSO PBS) for islet identification. Pure hand-picked islets were dispersed via Cell Dissociation Solution Non-Enzymatic (Sigma-Aldrich) for 10 min at 37°C. Single cell suspensions were washed and treated with Fc block antibody (clone 2.4G2) conditioned media (PBS, 1% bovine serum albumin, 0.1% $NaN_3$, and 10% 2.4G2 in DMEM) at 4°C for 15 min. Cells were then stained with fluorescent antibodies for flow cytometry and for sorting. Whole islet evaluation by immunofluorescence for total number of CD11c$^+$ cells and islet area was performed by first incubating 50–100 isolated islets in 50 µl DMEM with 10% FCS plus Fc block antibody for 15 min at 4°C, followed by a second incubation on ice for 45 min using 40 µg/ml anti-CD11c (N418; BioLegend). Islets were finally washed free of the antibody and fixed in 2% paraformaldehyde before examination.

**Antibodies for flow cytometry and cell sorting.** Flow cytometry was performed using a FACSCanto II (BD), and data were analyzed using FlowJo X software (Tree Star). Cell sorting was performed using a FACSAria II (BD). The following antibodies were purchased from BioLegend: BV510 anti-CD45 (30-F11), Pacific Blue (PB) anti–I-A/I-E (pan MHC-II), FITC anti-CD4 (RM4-5), (M5/114.15.2), APC and PerCP-Cy5.5 anti-F4/80 (BM8), PE-Cy7 anti-CD11b (M1/70), APC-Cy7 and Alexa Fluor 488 anti-CD11c (N418), PE anti-CD103 (2E7), PerCP-Cy5.5 anti-Ly6C (AL-21), PerCP-Cy5.5 anti-B220 (RA3-6B2), Alexa Fluor 647 (551), FITC anti-CD8α (53-6.7), PB anti-Ly6G (1A8), APC anti-CD64 (X54-5/7/1), Alexa Fluor 647 anti-CD68 (FA-11), PE anti-CD19 (1D3), PB anti-CD45.1

(A20), PerCP-Cy5.5 anti-CD45.2 (104), PE anti-NK1.1 (PK136), FITC anti–IL-7Rα (A7R34), Alexa Fluor 488 anti-CD206 (C068C2), and PE and PB anti-CD301 (LOM-14). For sorting stroma macrophages, pancreatic stroma was first incubated with PE anti-CD45 (BM8), APC anti-F4/80 (BM8), and Alexa Fluor 488 anti-CD206 from BioLegend for 30 min at 4°C and then enriched using the EasySep PE Positive Selection kit (STEMCELL Technologies) according to the manufacturer's protocol, with a few modifications to maintain cell viability (anti-PE cocktail incubation for 30 min at 4°C and magnetic nanoparticles incubation for 20 min at 4°C). For intracellular staining, Cytofix/Cytoperm and Perm/Wash buffer (BD) were used according to the manufacturer's protocol. APC anti-BrdU was purchased from BD and used according to the manufacturer's instructions.

**RNA isolation and real-time PCR.** Total RNA from sorted islet cells was isolated using the Ambion RNAqueous-Micro kit (Life Technologies) according to the manufacturer's instructions. RNA was quantified by OD260 using NanoDrop (Thermo Fisher Scientific; Ferris et al., 2014). cDNA was made from total RNA using TaqMan Reverse Transcription Reagents (Life Technologies) according to the random hexamer protocol. Primers for quantitative RT-PCR (qRT-PCR) were designed using the PrimeTime predesigned qPCR assays (IDT DNA). PrimeTime primers used 5′-nuclease detection technology and Primer Bank primers used SYBR Green I detection technology. PCR was performed using SSOFast Probes Supermix (Bio-Rad Laboratories) on a StepOnePlus Real-Time PCR system running StepOne Software (Applied Biosystems). Quality control and relative expression quantification for qPCR were performed by the StepOne 2.1 software.

**APC assay.** Islet macrophages and sorted $CD206^+$ and $CD206^-$ stroma macrophages were culture in DMEM + 10% FCS. 10 mice were pooled and the assay was run in duplicate. $2 \times 10^4$ cells were plated and incubated with LLO peptide (190–201) or a nonhemolytic variant of the LLO protein (LLOWW) for 2 h at 37°C (Carrero et al., 2012). $2 \times 10^5$ irradiated splenocytes served as positive controls. LLO antigen–specific (190–201) T cell hybridoma ($5 \times 10^4$ cells) was added for ∼16 h. Culture supernatants were tested for IL-2 production by CTLL-2 proliferation assay using $[^3H]$thymidine incorporation and expressed in counts per minute. All antigen presentation assays were performed in 200-µl final volume in 96-well tissue culture–coated flat-bottom plates (Corning).

**Statistical analysis.** Mann–Whitney *U* test or Student's *t* test was used to determine the level of significant differences between samples. Statistics were calculated and data were plotted using Prism 6 (GraphPad Software).

**Online supplemental material.** Fig. S1 shows islet gating strategy and examination. Fig. S2 shows stroma evaluation of $F4/80^-$ $CD11b^-$ leukocytes. Fig. S3 shows mouse models to evaluate ontogeny of pancreatic macrophages. Fig. S4 shows the multiple origins of pancreatic macrophages and their maintenance. Online supplemental material is available at http://www.jem.org/cgi/content/full/jem.20150496/DC1.

We are grateful to members of the laboratory for constructive discussions. Katherine Fredericks provided invaluable assistance with mouse handling. Liping Yang gave us technical assistance and advice with the parabiosis experiments.

Our research was supported by National Institutes of Health grants DK058177, DK020579, and P30DK020579 and by Juvenile Diabetes Research Foundation (JDRF) grant 17-2012-141.

The authors declare no competing financial interests.

**Submitted: 17 March 2015**
**Accepted: 11 August 2015**

## REFERENCES

Ajami, B., J.L. Bennett, C. Krieger, K.M. McNagny, and F.M. Rossi. 2011. Infiltrating monocytes trigger EAE progression, but do not contribute to the resident microglia pool. *Nat. Neurosci.* 14:1142–1149. http://dx.doi.org/10.1038/nn.2887

Bain, C.C., A. Bravo-Blas, C.L. Scott, E. Gomez Perdiguero, F. Geissmann, S. Henri, B. Malissen, L.C. Osborne, D. Artis, and A.M. Mowat. 2014. Constant replenishment from circulating monocytes maintains the macrophage pool in the intestine of adult mice. *Nat. Immunol.* 15:929–937. http://dx.doi.org/10.1038/ni.2967

Banaei-Bouchareb, L., V. Gouon-Evans, D. Samara-Boustani, M.C. Castellotti, P. Czernichow, J.W. Pollard, and M. Polak. 2004. Insulin cell mass is altered in *Csf1*$^{op}$/*Csf1*$^{op}$ macrophage-deficient mice. *J. Leukoc. Biol.* 76:359–367. http://dx.doi.org/10.1189/jlb.1103591

Böiers, C., N. Buza-Vidas, C.T. Jensen, C.J. Pronk, S. Kharazi, L. Wittmann, E. Sitnicka, A. Hultquist, and S.E. Jacobsen. 2010. Expression and role of FLT3 in regulation of the earliest stage of normal granulocyte-monocyte progenitor development. *Blood.* 115:5061–5068. http://dx.doi.org/10.1182/blood-2009-12-258756

Boyer, S.W., A.V. Schroeder, S. Smith-Berdan, and E.C. Forsberg. 2011. All hematopoietic cells develop from hematopoietic stem cells through Flk2/Flt3-positive progenitor cells. *Cell Stem Cell.* 9:64–73. http://dx.doi.org/10.1016/j.stem.2011.04.021

Boyer, S.W., A.E. Beaudin, and E.C. Forsberg. 2012. Mapping differentiation pathways from hematopoietic stem cells using Flk2/Flt3 lineage tracing. *Cell Cycle.* 11:3180–3188. http://dx.doi.org/10.4161/cc.21279

Buza-Vidas, N., P. Woll, A. Hultquist, S. Duarte, M. Lutteropp, T. Bouriez-Jones, H. Ferry, S. Luc, and S.E. Jacobsen. 2011. FLT3 expression initiates in fully multipotent mouse hematopoietic progenitor cells. *Blood.* 118:1544–1548. http://dx.doi.org/10.1182/blood-2010-10-316232

Calderon, B., A. Suri, M.J. Miller, and E.R. Unanue. 2008. Dendritic cells in islets of Langerhans constitutively present β cell-derived peptides bound to their class II MHC molecules. *Proc. Natl. Acad. Sci. USA.* 105:6121–6126. http://dx.doi.org/10.1073/pnas.0801973105

Calderon, B., J.A. Carrero, and E.R. Unanue. 2014. The central role of antigen presentation in islets of Langerhans in autoimmune diabetes. *Curr. Opin. Immunol.* 26:32–40. http://dx.doi.org/10.1016/j.coi.2013.10.011

Carrero, J.A., H. Vivanco-Cid, and E.R. Unanue. 2012. Listeriolysin O is strongly immunogenic independently of its cytotoxic activity. *PLoS ONE.* 7:e32310. http://dx.doi.org/10.1371/journal.pone.0032310

Chu, G.C., A.C. Kimmelman, A.F. Hezel, and R.A. DePinho. 2007. Stromal biology of pancreatic cancer. *J. Cell. Biochem.* 101:887–907. http://dx.doi.org/10.1002/jcb.21209

Clark, C.E., S.R. Hingorani, R. Mick, C. Combs, D.A. Tuveson, and R.H. Vonderheide. 2007. Dynamics of the immune reaction to pancreatic cancer from inception to invasion. *Cancer Res.* 67:9518–9527. http://dx.doi.org/10.1158/0008-5472.CAN-07-0175

Cucak, H., L.G. Grunnet, and A. Rosendahl. 2014. Accumulation of M1-like macrophages in type 2 diabetic islets is followed by a systemic shift in macrophage polarization. *J. Leukoc. Biol.* 95:149–160. http://dx.doi.org/10.1189/jlb.0213075

DeFalco, T., I. Bhattacharya, A.V. Williams, D.M. Sams, and B. Capel. 2014. Yolk-sac–derived macrophages regulate fetal testis vascularization and morphogenesis. *Proc. Natl. Acad. Sci. USA.* 111:E2384–E2393. http://dx.doi.org/10.1073/pnas.1400057111

Ehses, J.A., A. Perren, E. Eppler, P. Ribaux, J.A. Pospisilik, R. Maor-Cahn, X. Gueripel, H. Ellingsgaard, M.K. Schneider, G. Biollaz, et al. 2007. Increased number of islet-associated macrophages in type 2 diabetes. *Diabetes.* 56:2356–2370. http://dx.doi.org/10.2337/db06-1650

Epelman, S., K.J. Lavine, A.E. Beaudin, D.K. Sojka, J.A. Carrero, B. Calderon, T. Brija, E.L. Gautier, S. Ivanov, A.T. Satpathy, et al. 2014a. Embryonic and adult-derived resident cardiac macrophages are maintained through distinct mechanisms at steady state and during inflammation. *Immunity.* 40:91–104. http://dx.doi.org/10.1016/j.immuni.2013.11.019

Epelman, S., K.J. Lavine, and G.J. Randolph. 2014b. Origin and functions of tissue macrophages. *Immunity.* 41:21–35. http://dx.doi.org/10.1016/j.immuni.2014.06.013

Ferrante, A.W. Jr. 2013. The immune cells in adipose tissue. *Diabetes Obes. Metab.* 15:34–38. http://dx.doi.org/10.1111/dom.12154

Ferris, S.T., J.A. Carrero, J.F. Mohan, B. Calderon, K.M. Murphy, and E.R. Unanue. 2014. A minor subset of Batf3-dependent antigen-presenting cells in islets of Langerhans is essential for the development of autoimmune diabetes. *Immunity.* 41:657–669. http://dx.doi.org/10.1016/j.immuni.2014.09.012

Gautier, E.L., T. Shay, J. Miller, M. Greter, C. Jakubzick, S. Ivanov, J. Helft, A. Chow, K.G. Elpek, S. Gordonov, et al. Immunological Genome Consortium. 2012. Gene-expression profiles and transcriptional regulatory pathways that underlie the identity and diversity of mouse tissue macrophages. *Nat. Immunol.* 13:1118–1128. http://dx.doi.org/10.1038/ni.2419

Geutskens, S.B., T. Otonkoski, M.A. Pulkkinen, H.A. Drexhage, and P.J. Leenen. 2005. Macrophages in the murine pancreas and their involvement in fetal endocrine development in vitro. *J. Leukoc. Biol.* 78:845–852. http://dx.doi.org/10.1189/jlb.1004624

Ginhoux, F., M. Greter, M. Leboeuf, S. Nandi, P. See, S. Gokhan, M.F. Mehler, S.J. Conway, L.G. Ng, E.R. Stanley, et al. 2010. Fate mapping analysis reveals that adult microglia derive from primitive macrophages. *Science.* 330:841–845. http://dx.doi.org/10.1126/science.1194637

Gordon, S., A. Plüddemann, and F. Martinez Estrada. 2014. Macrophage heterogeneity in tissues: phenotypic diversity and functions. *Immunol. Rev.* 262:36–55. http://dx.doi.org/10.1111/imr.12223

Gosselin, D., V.M. Link, C.E. Romanoski, G.J. Fonseca, D.Z. Eichenfield, N.J. Spann, J.D. Stender, H.B. Chun, H. Garner, F. Geissmann, and C.K. Glass. 2014. Environment drives selection and function of enhancers controlling tissue-specific macrophage identities. *Cell.* 159:1327–1340. http://dx.doi.org/10.1016/j.cell.2014.11.023

Guilliams, M., I. De Kleer, S. Henri, S. Post, L. Vanhoutte, S. De Prijck, K. Deswarte, B. Malissen, H. Hammad, and B.N. Lambrecht. 2013. Alveolar macrophages develop from fetal monocytes that differentiate into long-lived cells in the first week of life via GM-CSF. *J. Exp. Med.* 210:1977–1992.

Haniffa, M., F. Ginhoux, X.N. Wang, V. Bigley, M. Abel, I. Dimmick, S. Bullock, M. Grisotto, T. Booth, P. Taub, et al. 2009. Differential rates of replacement of human dermal dendritic cells and macrophages during hematopoietic stem cell transplantation. *J. Exp. Med.* 206:371–385. http://dx.doi.org/10.1084/jem.20081633

Hashimoto, D., A. Chow, C. Noizat, P. Teo, M.B. Beasley, M. Leboeuf, C.D. Becker, P. See, J. Price, D. Lucas, et al. 2013. Tissue-resident macrophages self-maintain locally throughout adult life with minimal contribution from circulating monocytes. *Immunity.* 38:792–804. http://dx.doi.org/10.1016/j.immuni.2013.04.004

Hoeffel, G., Y. Wang, M. Greter, P. See, P. Teo, B. Malleret, M. Leboeuf, D. Low, G. Oller, F. Almeida, et al. 2012. Adult Langerhans cells derive predominantly from embryonic fetal liver monocytes with a minor contribution of yolk sac–derived macrophages. *J. Exp. Med.* 209:1167–1181. http://dx.doi.org/10.1084/jem.20120340

Hume, D.A., D. Halpin, H. Charlton, and S. Gordon. 1984. The mononuclear phagocyte system of the mouse defined by immunohistochemical localization of antigen F4/80: macrophages of endocrine organs. *Proc. Natl. Acad. Sci. USA.* 81:4174–4177. http://dx.doi.org/10.1073/pnas.81.13.4174

Ino, K., M. Masuya, I. Tawara, E. Miyata, K. Oda, Y. Nakamori, K. Suzuki, K. Ohishi, and N. Katayama. 2014. Monocytes infiltrate the pancreas via the MCP-1/CCR2 pathway and differentiate into stellate cells. *PLoS ONE.* 9:e84889. http://dx.doi.org/10.1371/journal.pone.0084889

Kumaravelu, P., L. Hook, A.M. Morrison, J. Ure, S. Zhao, S. Zuyev, J. Ansell, and A. Medvinsky. 2002. Quantitative developmental anatomy of definitive haematopoietic stem cells/long-term repopulating units (HSC/RUs): role of the aorta-gonad-mesonephros (AGM) region and the yolk sac in colonisation of the mouse embryonic liver. *Development.* 129:4891–4899.

Lavin, Y., D. Winter, R. Blecher-Gonen, E. David, H. Keren-Shaul, M. Merad, S. Jung, and I. Amit. 2014. Tissue-resident macrophage enhancer landscapes are shaped by the local microenvironment. *Cell.* 159:1312–1326. http://dx.doi.org/10.1016/j.cell.2014.11.018

Lewis, K.L., M.L. Caton, M. Bogunovic, M. Greter, L.T. Grajkowska, D. Ng, A. Klinakis, I.F. Charo, S. Jung, J.L. Gommerman, et al. 2011. Notch2 receptor signaling controls functional differentiation of dendritic cells in the spleen and intestine. *Immunity.* 35:780–791. http://dx.doi.org/10.1016/j.immuni.2011.08.013

Li, D.S., Y.H. Yuan, H.J. Tu, Q.L. Liang, and L.J. Dai. 2009. A protocol for islet isolation from mouse pancreas. *Nat. Protoc.* 4:1649–1652. http://dx.doi.org/10.1038/nprot.2009.150

Lichanska, A.M., and D.A. Hume. 2000. Origins and functions of phagocytes in the embryo. *Exp. Hematol.* 28:601–611. http://dx.doi.org/10.1016/S0301-472X(00)00157-0

Lichanska, A.M., C.M. Browne, G.W. Henkel, K.M. Murphy, M.C. Ostrowski, S.R. McKercher, R.A. Maki, and D.A. Hume. 1999. Differentiation of the mononuclear phagocyte system during mouse embryogenesis: the role of transcription factor PU.1. *Blood.* 94:127–138.

Lin, H., E. Lee, K. Hestir, C. Leo, M. Huang, E. Bosch, R. Halenbeck, G. Wu, A. Zhou, D. Behrens, et al. 2008. Discovery of a cytokine and its receptor by functional screening of the extracellular proteome. *Science.* 320:807–811. http://dx.doi.org/10.1126/science.1154370

Lumeng, C.N., J.L. Bodzin, and A.R. Saltiel. 2007. Obesity induces a phenotypic switch in adipose tissue macrophage polarization. *J. Clin. Invest.* 117:175–184. http://dx.doi.org/10.1172/JCI29881

Melli, K., R.S. Friedman, A.E. Martin, E.B. Finger, G. Miao, G.L. Szot, M.F. Krummel, and Q. Tang. 2009. Amplification of autoimmune response through induction of dendritic cell maturation in inflamed tissues. *J. Immunol.* 182:2590–2600. http://dx.doi.org/10.4049/jimmunol.0803543

Merad, M., P. Sathe, J. Helft, J. Miller, and A. Mortha. 2013. The dendritic cell lineage: ontogeny and function of dendritic cells and their subsets in the steady state and the inflamed setting. *Annu. Rev. Immunol.* 31:563–604. http://dx.doi.org/10.1146/annurev-immunol-020711-074950

Meredith, M.M., K. Liu, G. Darrasse-Jeze, A.O. Kamphorst, H.A. Schreiber, P. Guermonprez, J. Idoyaga, C. Cheong, K.H. Yao, R.E. Niec, and M.C. Nussenzweig. 2012. Expression of the zinc finger transcription factor zDC (Zbtb46, Btbd4) defines the classical dendritic cell lineage. *J. Exp. Med.* 209:1153–1165. http://dx.doi.org/10.1084/jem.20112675

Mohan, J.F., M.G. Levisetti, B. Calderon, J.W. Herzog, S.J. Petzold, and E.R. Unanue. 2010. Unique autoreactive T cells recognize insulin peptides generated within the islets of Langerhans in autoimmune diabetes. *Nat. Immunol.* 11:350–354. http://dx.doi.org/10.1038/ni.1850

Molawi, K., Y. Wolf, P.K. Kandalla, J. Favret, N. Hagemeyer, K. Frenzel, A.R. Pinto, K. Klapproth, S. Henri, B. Malissen, et al. 2014. Progressive replacement of embryo-derived cardiac macrophages with age. *J. Exp. Med.* 211:2151–2158. http://dx.doi.org/10.1084/jem.20140639

Murray, P.J., and T.A. Wynn. 2011. Protective and pathogenic functions of macrophage subsets. *Nat. Rev. Immunol.* 11:723–737. http://dx.doi.org/10.1038/nri3073

Murray, P.J., J.E. Allen, S.K. Biswas, E.A. Fisher, D.W. Gilroy, S. Goerdt, S. Gordon, J.A. Hamilton, L.B. Ivashkiv, T. Lawrence, et al. 2014. Macrophage activation and polarization: nomenclature and experimental guidelines. *Immunity.* 41:14–20. http://dx.doi.org/10.1016/j.immuni.2014.06.008

Peng, H., X. Jiang, Y. Chen, D.K. Sojka, H. Wei, X. Gao, R. Sun, W.M. Yokoyama, and Z. Tian. 2013. Liver-resident NK cells confer adaptive immunity in skin-contact inflammation. *J. Clin. Invest.* 123:1444–1456. http://dx.doi.org/10.1172/JCI66381

Pinto, A.R., R. Paolicelli, E. Salimova, J. Gospocic, E. Slonimsky, D. Bilbao-Cortes, J.W. Godwin, and N.A. Rosenthal. 2012. An abundant tissue macrophage population in the adult murine heart with a distinct alternatively-activated macrophage profile. *PLoS ONE.* 7:e36814. http://dx.doi.org/10.1371/journal.pone.0036814

Pollard, J.W., M.G. Dominguez, S. Mocci, P.E. Cohen, and E.R. Stanley. 1997. Effect of the colony-stimulating factor-1 null mutation, osteopetrotic (csfm(op)), on the distribution of macrophages in the male mouse reproductive tract. *Biol. Reprod.* 56:1290–1300. http://dx.doi.org/10.1095/biolreprod56.5.1290

Richardson, S.J., A. Willcox, A.J. Bone, A.K. Foulis, and N.G. Morgan. 2009. Islet-associated macrophages in type 2 diabetes. *Diabetologia.* 52:1686–1688. http://dx.doi.org/10.1007/s00125-009-1410-z

Salvalaggio, P.R., S. Deng, C.E. Ariyan, I. Millet, W.S. Zawalich, G.P. Basadonna, and D.M. Rothstein. 2002. Islet filtration: a simple and rapid new purification procedure that avoids ficoll and improves islet mass and function. *Transplantation.* 74:877–879. http://dx.doi.org/10.1097/00007890-200209270-00023

Satpathy, A.T., W. Kc, J.C. Albring, B.T. Edelson, N.M. Kretzer, D. Bhattacharya, T.L. Murphy, and K.M. Murphy. 2012. Zbtb46 expression distinguishes classical dendritic cells and their committed progenitors from other immune lineages. *J. Exp. Med.* 209:1135–1152. http://dx.doi.org/10.1084/jem.20120030

Satpathy, A.T., C.G. Briseño, J.S. Lee, D. Ng, N.A. Manieri, W. Kc, X. Wu, S.R. Thomas, W.L. Lee, M. Turkoz, et al. 2013. Notch2-dependent classical dendritic cells orchestrate intestinal immunity to attaching-and-effacing bacterial pathogens. *Nat. Immunol.* 14:937–948. http://dx.doi.org/10.1038/ni.2679

Schulz, C., E. Gomez Perdiguero, L. Chorro, H. Szabo-Rogers, N. Cagnard, K. Kierdorf, M. Prinz, B. Wu, S.E. Jacobsen, J.W. Pollard, et al. 2012. A lineage of myeloid cells independent of Myb and hematopoietic stem cells. *Science*. 336:86–90. http://dx.doi.org/10.1126/science.1219179

Serbina, N.V., and E.G. Pamer. 2006. Monocyte emigration from bone marrow during bacterial infection requires signals mediated by chemokine receptor CCR2. *Nat. Immunol.* 7:311–317. http://dx.doi.org/10.1038/ni1309

Shaul, M.E., G. Bennett, K.J. Strissel, A.S. Greenberg, and M.S. Obin. 2010. Dynamic, M2-like remodeling phenotypes of CD11c+ adipose tissue macrophages during high-fat diet–induced obesity in mice. *Diabetes*. 59:1171–1181. http://dx.doi.org/10.2337/db09-1402

Sica, A., and A. Mantovani. 2012. Macrophage plasticity and polarization: in vivo veritas. *J. Clin. Invest.* 122:787–795. http://dx.doi.org/10.1172/JCI59643

Sojka, D.K., B. Plougastel-Douglas, L. Yang, M.A. Pak-Wittel, M.N. Artyomov, Y. Ivanova, C. Zhong, J.M. Chase, P.B. Rothman, J. Yu, et al. 2014. Tissue-resident natural killer (NK) cells are cell lineages distinct from thymic and conventional splenic NK cells. *eLife*. 3:e01659. http://dx.doi.org/10.7554/eLife.01659

Spits, H., D. Artis, M. Colonna, A. Diefenbach, J.P. Di Santo, G. Eberl, S. Koyasu, R.M. Locksley, A.N. McKenzie, R.E. Mebius, et al. 2013. Innate lymphoid cells—a proposal for uniform nomenclature. *Nat. Rev. Immunol.* 13:145–149. http://dx.doi.org/10.1038/nri3365

Wang, Y., K.J. Szretter, W. Vermi, S. Gilfillan, C. Rossini, M. Cella, A.D. Barrow, M.S. Diamond, and M. Colonna. 2012. IL-34 is a tissue-restricted ligand of CSF1R required for the development of Langerhans cells and microglia. *Nat. Immunol.* 13:753–760. http://dx.doi.org/10.1038/ni.2360

Westwell-Roper, C.Y., J.A. Ehses, and C.B. Verchere. 2014. Resident macrophages mediate islet amyloid polypeptide-induced islet IL-1β production and β-cell dysfunction. *Diabetes*. 63:1698–1711. http://dx.doi.org/10.2337/db13-0863

Xiao, X., I. Gaffar, P. Guo, J. Wiersch, S. Fischbach, L. Peirish, Z. Song, Y. El-Gohary, K. Prasadan, C. Shiota, and G.K. Gittes. 2014. M2 macrophages promote beta-cell proliferation by up-regulation of SMAD7. *Proc. Natl. Acad. Sci. USA*. 111:E1211–E1220. http://dx.doi.org/10.1073/pnas.1321347111

Yin, N., N. Zhang, G. Lal, J. Xu, M. Yan, Y. Ding, and J.S. Bromberg. 2011. Lymphangiogenesis is required for pancreatic islet inflammation and diabetes. *PLoS ONE*. 6:e28023. http://dx.doi.org/10.1371/journal.pone.0028023

Yona, S., K.W. Kim, Y. Wolf, A. Mildner, D. Varol, M. Breker, D. Strauss-Ayali, S. Viukov, M. Guilliams, A. Misharin, et al. 2013. Fate mapping reveals origins and dynamics of monocytes and tissue macrophages under homeostasis. *Immunity*. 38:79–91. http://dx.doi.org/10.1016/j.immuni.2012.12.001